
Introduction

1

1. MOTIVATION OF THE STUDY

The optical system of the eye is formed by the cornea and the crystalline lens, which project the images of the outside world on the retina. A scheme of the eye is depicted in Figure 1.1. In the last few years there has been an increased interest in the assessment of the optical quality of the normal eye (Castejon-Mochon, Lopez-Gil, Benito & Artal, 2002, Marcos, Burns, Prieto, Navarro & Baraibar, 2001), as well as the changes of optical quality with certain conditions such as aging (McLellan, Marcos & Burns, 2001), accommodation (He, Burns & Marcos, 2000) and refractive errors (Llorente, Barbero, Cano, Dorronsoro & Marcos, 2004), and particularly how the optical aberrations are modified after certain interventions such as refractive surgery (Moreno-Barriuso, Merayo-Llodes, Marcos, Navarro, Llorente & Barbero, 2001), intraocular surgery (Barbero, Marcos & Jimenez-Alfaro, 2003) and contact lenses (Dorronsoro, Barbero, Llorente & Marcos, 2003). While there is a good description of the ocular aberrations of the eye, driven by the development of reliable aberrometers (Marcos, Burns, Moreno-Barriuso & Navarro, 1999), the sources of the aberrations in individual eyes and their changes associated with different conditions are not well understood. The anterior cornea is the most powerful refractive surface in the eye (due in part to the change in the refractive index between air and corneal surface). Measurements of the corneal elevation maps allow estimation of the contribution of anterior corneal aberrations to the ocular aberrations. However, the contribution of the crystalline lens to the overall optical quality of the eye is not well understood. First, the crystalline lens is not that easily accessible *in vivo* as the corneal surface, as it needs to be imaged through different ocular surfaces which produce optical distortions. Second, the geometry of the lens changes dynamically with accommodation (Dubbelman, van der Heijde & Weeber, 2005, Fincham, 1925, Kirschkamp, Dunne & Barry, 2004, Koretz, Cook & Kaufman, 2002, Koretz, Handelman & Brown, 1984, Strenk, Strenk, Semmlow & DeMarco, 2004). Third, the index of refraction of the lens is not homogenous, as it shows a gradient index distribution (Atchison & Smith, 1995, Dick, 1994, Dubbelman & van der Heijde, 2001, Garner & Smith, 1997, Mutti, Zadnik, Fusaro, Friedman, Sholtz & Adams, 1998, Pierscionek, 1997, Smith & Atchison, 2001). And forth, the crystalline lens grows throughout life and its shape and structure experiences important changes with age (Brown, 1974, Dubbelman & van der Heijde, 2001, Dubbelman, van der Heijde & Weeber, 2001, Garner, Ooi & Smith, 1998, Glasser & Campbell, 1998,

Introduction

Hemenger, Garner & Ooi, 1995, Kasthurirangan, Markwell, Atchison, Pope & Smith, 2007, Koretz, Cook & Kaufman, 1997, Koretz, Cook & Kaufman, 2001, Smith, Atchison & Pierscionek, 1992, Strenk et al., 2004).

Apart from the optical properties of the “isolated” optical components, the interactions between cornea and crystalline lens, and their relative positioning, are critical to understand the overall quality in the eye. Measurements of total and corneal aberrations have demonstrated that in the normal young eye the aberrations of the crystalline lens partially balance those of the cornea. A better understanding of the structural properties of the crystalline lens will help to better understand how this is achieved. While there have been attempts to relate the presence of asymmetric aberrations such as coma to the tilt of the optical axis (Marcos et al., 2001), the lack of precise measurements of geometry and positioning (tilt and decentration) of the crystalline lens in the past have prevented full understanding the contributions of internal optics to the ocular aberrations. In particular, there is an open debate on the active (Kelly, Mihashi & Howland, 2004) or passive (Artal, Benito & Tabenero, 2006) nature of this compensation mechanism on which accurate measurements of individual structural properties in eyes will shed light.

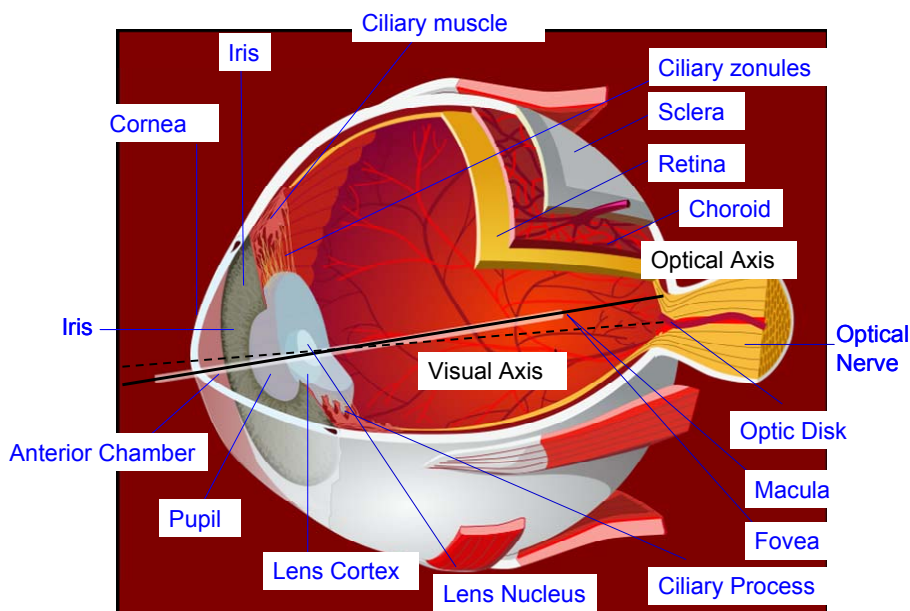


Figure 1.1. Scheme of the human eye's anatomy.

One of the most extraordinary capabilities of the human eye is the ability to focus near and far objects. This accommodation capacity is progressively lost with age affecting performance in near tasks (presbyopia). While this condition affects 100% of the population beyond 45 years, the mechanism that leads to presbyopia is not well understood (Glasser & Campbell, 1999, Glasser, Croft & Kaufman, 2001, Koretz et al., 1997, Lewis, 1983, Spierer & Shalev, 2003, Strenk, Strenk & Koretz, 2005). While it is well known that the crystalline lens changes its shape to accommodate, the data regarding the change of the lens shape with accommodation in literature are controversial, with discrepancies arising from differences between in vivo and in vitro accommodative states and potentially the use of imaging techniques not fully correcting for distortion. An accurate knowledge of the changes in shape with accommodation is critical to assess the relative contribution of surface power and gradient index distribution (not covered in this thesis) to the accommodative amplitude, and to understanding the optical aberrations of the crystalline lens. In addition, the change in tilt and decentration of the crystalline lens with accommodation has never been addressed in depth. To our knowledge there is only one study of changes in tilt and decentration of the crystalline lens with accommodation using the Purkinje imaging technique (Kirschkamp et al., 2004). Fully characterizing the accommodative mechanism is essential to understanding the progression of presbyopia, and to aid in strategies to correct presbyopia, i.e., for the design of accommodative intraocular lenses (Küchle, Seitz, Langenbacher & et al, 2004, Stachs, Schneider, Stave & Guthoff, 2005), lens refilling (Koopmans, Terwee, Glasser, Wendt, Vilupuru, van Kooten & et al, 2006, Norrby, Koopmans & Terwee, 2006), chemical laser treatment of the lens (Krueger, Seiler, Gruchman, Mrochen & Berlin, 2001, Myers & Krueger, 1998), and other surgical procedures (Qazi, Pepose & Shuster, 2002).

When the crystalline lens becomes opaque with aging, it is generally surgically removed and replaced by an intraocular lens. Cataract surgery has benefited from technical advances that allow smaller corneal incisions (leading to less incision-induced corneal aberrations) and continuous improvements of intraocular lens design (Marcos et al., 2005). However, customization of cataract surgery will be ultimately limited by the IOL design and IOL positioning. The study of the contributions to optical quality of corneal aberrations, intraocular lens design, intraocular lens tilt and decentration, particularly in combination with measurements of ocular aberrations, are very valuable to evaluate the actual performance of a given IOL design and to guide new designs.

In brief, this thesis addresses novel and validated in vivo measurements on eyes with intact crystalline lenses and pseudophakic eyes with intraocular lenses, which will contribute to the understanding of the image forming capabilities of the eye (particularly the lens), the optical changes in the crystalline lens with accommodation and optical performance after cataract surgery.

2. THE CRYSTALLINE LENS AND THE ACCOMMODATIVE SYSTEM

2.1 Human and primate crystalline lens

2.1.1. Human crystalline lens

The crystalline lens is a unique transparent, biconvex intraocular structure that lies in the anterior segment of the eye, suspended radially at its equator by the zonular fibers and ciliary body between the iris and the vitreous body. Enclosed in an elastic capsule, the lens has no innervation or blood supply after fetal development. Its nourishment must be obtained from the surrounding aqueous and vitreous that is thought to provide support and stabilization for the posterior surface of the lens, and the same media must also remove metabolic waste products. The aqueous humor continuously flows from the ciliary body to the anterior chamber, bathing the anterior surface of the lens. The lateral border of the lens is the equator, formed from the joining of the anterior and posterior capsules, and is the site of insertion of the zonules.

The anterior and posterior lens surface curvatures are usually described as aspherical in shape. Some authors report a steeper curvature located centrally near the optical axis with the surfaces becoming progressively flatter toward the midperiphery and then steeper toward the equatorial edges (Dubbelman & van der Heijde, 2001). This aspherical anterior and posterior lens surface tends to minimize spherical aberration. The magnitude of lens curvature, and particularly the change of curvature with accommodation and aging has been a matter of long debate in the literature. These measurements will be addressed in Chapters 4 and 6. The most recent measurements of lens asphericity in vivo by Dubbelman (Dubbelman et al., 2005) show large intersubject variability.

The crystalline lens is composed of multiple layers of long, fiber cells that originate from the equator and stretch toward the poles of the lens. At the point where the cells meet, they form suture patterns. In the human, the embryonic lens has “Y” sutures, but

as it ages, the suture patterns in the new layers become increasingly more complex, resulting in a lens whose suture patterns have a starlike appearance (Koretz, Cook & Kuszak, 1994).

The lens consists of three components: capsule, epithelium, and lens substance. The lens substance is a product of the continuous growth of the epithelium and consists of the cortex and nucleus. The transition between the cortex and nucleus is gradual. There is no a concise line of demarcation when observed in histological sections. The lines of demarcation are often better visualized by slit-lamp microscopy.

The lens capsule is a basement membrane formed of the lens epithelium anteriorly and by superficial fibers posteriorly. With light microscopy, the lens capsule appears as a structureless, elastic membrane that completely surrounds the lens. The capsule functions as a metabolic barrier and may play a role in lens shaping during accommodation. The lens capsule is of variable thickness being much thicker in the anterior than the posterior capsule.

The lens epithelium is confined to the anterior surface and the equatorial lens bow. It consists of a single row of cuboidal-cylindrical cells, which can biologically be divided into two different zones with two different types of cells: *A-cells*, located in the central zone of the anterior lens capsule, with minimal mitotic activity and rarely migrating; *E-cells*, located in the second zone as a continuation of the anterior lens epithelial cells around the equator and responsible for the continuous formation of all cortical fibers, in early life, nuclear fibers, and therefore accounting for the continuous growth in size and weight of the lens throughout life. During lens enlargement, the location of older fibers becomes relatively more central as new fibers are formed at the periphery.

The lens cortex and nucleus consists of the lens fibers themselves. On cross-section, these cells are hexagonal and bound together by ground substance. After formation, the cellular nuclei of the lens fibers are present only temporarily. Subsequently, they disappear, leaving the lens center devoid of cell nuclei. The most peripherally located fibers, which underlie the lens capsule, form the lens cortex once the nucleus is completed. The designation of cortex is actually an arbitrary term signifying a peripheral location within the lens, rather than specific fibers.

Figure 1.2 shows images of the crystalline lens in vitro, in a postmortem phakic human eye (A), and the anatomical relationship of the human crystalline lens, ciliary body, and zonules, viewed at higher magnification (B), from a study by Pandey (Pandey, Wilson & Trivedi, 2001). The human ciliary body extends from the base of the

Introduction

iris to become continuous with the choroid at the ora serrata. Histologically, the human ciliary body consists of seven layers, one of which is the ciliary muscle. In accommodation, contraction of the ciliary muscle releases zonular tension on the crystalline lens, which allows the lens to assume a more spherical shape, thereby increasing the power of the eye.

The ciliary zonules consist essentially of a series of fibers passing from the ciliary body to the lens. They hold the lens in position and enable the ciliary muscle to act on the lens during accommodation. The lens and zonules form a diaphragm, which divide the eye into a smaller anterior portion and a larger posterior portion. The zonule forms a ring, which is roughly triangular in a meridional section. The base of the triangle is concave and faces the equatorial edge of the lens.



Figure 1.2. Parasagittal section of a phakic human eye obtained postmortem. Note the crystalline lens suspended by the ciliary zonules. **A.** Crystalline lens and zonules. **B.** Higher magnification of crystalline lens, ciliary body, and zonules from another case. **C.** Higher magnification of ciliary body and zonules from another case, posterior view. Image adapted from Pandey (Glasser, Wendt & Ostrin, 2006, Pandey, Thakur, Werner, Wilson, Werner, Izak & Apple, 2002)

2.1.2. Primate Crystalline lens

Several studies have shown the similarity of the ocular anatomy and accommodative mechanism of the rhesus monkey and human. For example, the study by Kaufman on 108 monkey eyes after total iridectomy show that this is an appropriate model of human accommodation and presbyopia (Kaufman & Lütjen-Drecoll, 1975). Figure 1.3 shows images of isolated crystalline lenses obtained by shadowphotography (Augusteyn et al., 2006) on human eyes and rhesus monkeys, where typical dimensions can be compared. To make ages comparable in the human and rhesus monkey ages the following expression must be taken into account: $\text{human_years} = 1.3846 * \text{monkey_years} + 10.385$ (Vilupuru & Glasser, 2002).

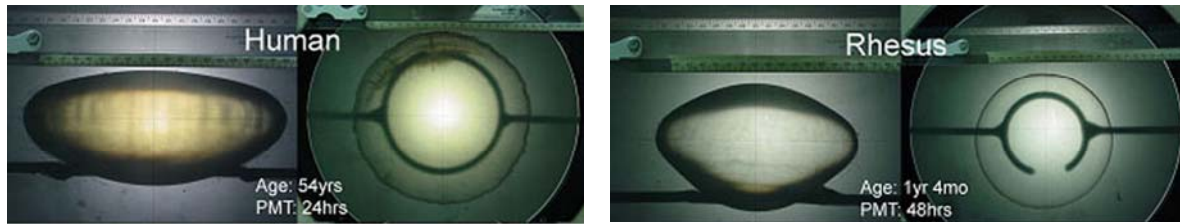


Figure 1. 3. Coronal and sagittal shadow photographs of a 54 years old human eye and a 1 and four months year old Rhesus Monkey. The lenses are shown with their anterior sides up and are magnified 20x relative to the ruler in the photograph. Images obtained by Augusteyn (Augusteyn, Rosen, Borja, Ziebarth & Parel, 2006).

Using a distortion-corrected Scheimpflug camera, LaPuerta & Schein (Lapuerta & Schein, 1995) measured the intraocular distances, and curvatures of the anterior and posterior cornea and lens of eight eyes of four monkey eyes (*Macaca fascicularis*). Table 1 compares biometric values of a human schematic eye (Le Grand full schematic eye (Le Grand & El Hage, 1980) Table 1.a) with the monkey schematic eye developed by Lapuerta and Schein (Table 1.b).

Table 1.a. Le Grand schematic human eye.

Medium	Refractive Index n	Radius of curvature R (mm)	Intraocular distances d (mm)
Air	1.0000		
Cornea	1.3771	7.80	0.55
		6.50	
Aqueous	1.3374		3.05
Lens	1.4200	10.20	4.00
		-6.00	
Vitreous	1.3360		16.59

Table 1.b. La Puerta schematic model eye.

Medium	n	R (mm)	d (mm)
Air	1.0000		
Anterior Cornea	1.3771	5.75	0.55
Posterior Cornea		5.12	
Aqueous	1.336		3.05
Anterior Lens	1.4200	10.34	4.00
Posterior Lens		-6.390	
Vitreous	1.3360		10.32

There are several studies of the similarity of the accommodative mechanism (Crawford, Kaufman & Bito, 1990, Glasser & Kaufman, 1999, McWhae & Reimer, 2000, Vilupuru & Glasser, 2002, Vilupuru & Glasser, 2003) and age dependent loss of accommodative amplitude in rhesus monkeys (Koretz, Bertasso, Neider & Kaufman PL, 1988, Koretz, Bertasso, Neider, True-Galbelt & Kaufman, 1987a, Koretz, Neider, Kaufman, Bertasso, DeRousseau & Bito, 1987c, Neider, Crawford, Kaufman & Bito, 1990). According to those studies, rhesus monkeys and humans exhibit a similar accommodative mechanism and lens growth throughout life and develop presbyopia with a similar relative age course, although differences between monkeys and human accommodation can be found in the extent to which presbyopia affects the various intraocular accommodative structures (Croft, Glasser & Kaufman, 2001).

2.2 The Accommodative Mechanism

Accommodation is an increase in the dioptric power of the eye that enables the image of near objects to be focused on the retina. The act of focusing the eye on objects at different distances includes far-to-near (accommodation) and near-to-far (disaccommodation) focus.

2.2.1 Different accommodative mechanism theories

According to the classic Helmholtz mechanism of accommodation theory (Von Helmholtz, 1855), during distant vision (when the lens is unaccommodated, Figure 1.4.A) the ciliary muscle is relaxed, the zonular fibers are under tension and the lens is pulled flat. During accommodation (Figure 1.4.B), the ciliary muscle contracts, releasing tension on the zonular fibers at the lens equator, allowing the lens equatorial diameter to decrease, the lens thickness to increase, and the lens surfaces to become more steeply curved.

Schachar (Schachar, Cudmore & Black, 1993) based on Thscherning's theory (Tscherning, 1904) postulated that with accommodation, ciliary muscle contraction causes a relaxation of the anterior and posterior zonular fibres, but an increased tension in the equatorial zonular fibres (Schachar, 1994), which cause the peripheral part of the lens to flatten, whereas the central part of the lens becomes more convex (increasing lens power). This theory erroneously relies on an increase of the equatorial lens diameter during accommodation, while it has been demonstrated that the equatorial diameter decreases with accommodation (Glasser et al., 2006).

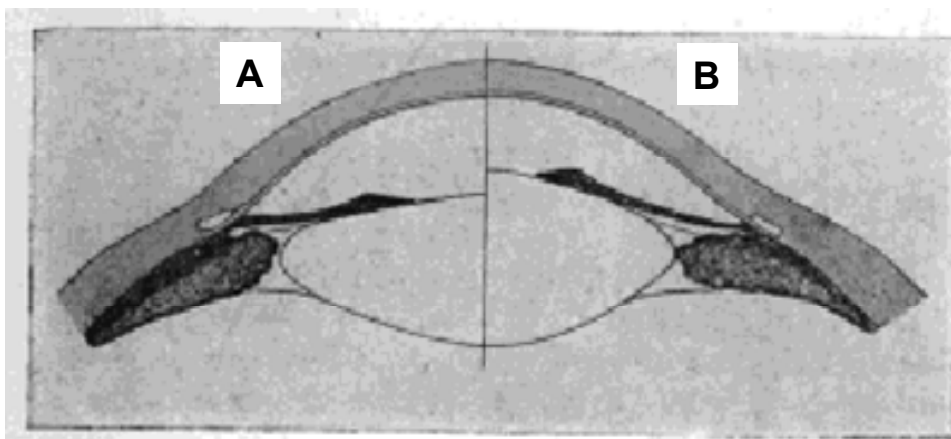


Figure 1.4. Helmholtz theory of accommodation. **A.** is a representation of the unaccommodated state of the lens, **B.** represents the accommodated state, where the ciliary muscle is contracted, so the tension of the zonular fibres is relaxed and the lens becomes more convex by virtue of its own elasticity (image adapted from <http://www.iblindness.org/books/bates/ch3.html>)

2.2.2 Biometric changes during accommodation

The study of biometric changes of the crystalline lens and ciliary body during dynamic accommodation is essential to understanding the mechanism of accommodation and age-related changes leading to presbyopia. The lenticular accommodative biometric data most widely available refer to axial changes in the anterior segment. Anterior movement of the anterior crystalline lens surface and an increase in lens thickness has been demonstrated in several studies, in both humans (Beers & van der Heijde, 1994a, Bolz, Prinz, Drexler & Findl, 2007, Dubbelman et al., 2005, Garner & Yap, 1997, Ostrin, Kasthurirangan, Win-Hall & Glasser, 2006, Zadnik, Mutti & Adams, 1992) and rhesus monkeys either drug stimulated (Koretz, Bertasso, Neider, True-Galbelt & Kaufman, 1987b) or centrally stimulated (Vilupuru & Glasser, 2005). Accommodative movement of the posterior lens surface has only recently become clear. Corrected Scheimpflug images show a posterior accommodative movement of the posterior lens surface (Dubbelman et al., 2005). Two recent studies in humans related measurements of anterior chamber depth, lens thickness and anterior segment length using A-scan ultrasonography or partial coherence interferometry with refraction measured simultaneously either in the same eye or in the contralateral eye (Bolz et al., 2007, Ostrin et al., 2006). These studies show an accommodative movement of the posterior lens surface. Similar results occur with centrally stimulated accommodation in rhesus monkeys (Vilupuru & Glasser, 2005). Changes in anterior and/or posterior lens curvature with accommodation in humans have been reported by several authors (Garner, 1983, Garner & Smith, 1997, Garner & Yap, 1997, Kirschkamp et al., 2004, Brown, 1973, Dubbelman et al., 2005, Koretz et al., 1987b, Koretz et al., 1984). The change in lens radii of curvature with accommodation will be discussed in depth in Chapter 4 and 6, and new data will be reported in this thesis, both in humans and iridectomized monkeys.

The use of iridectomized monkeys (Kaufman & Lütjen-Drecoll, 1975) has allowed measurements to be performed on lenticular regions generally not accessible with optical techniques in eyes with intact irides. For example, a decrease in lens equatorial diameter with increased accommodation (Glasser et al., 2006), as well as centripetal ciliary processes and lens edge movements have been demonstrated dynamically using slit-lamp goniovideography (Croft, Glasser, Heatley, McDonald, Ebbert, Nadkarni & Kaufman, 2006, Ostrin & Glasser, 2007). While axial changes in

lens position, and centripetal movements of the crystalline lens have been studied in detail, to our knowledge, only one human study has looked at possible changes in crystalline lens tilt and decentration (in the horizontal direction) for unaccommodated and accommodated eyes (Kirschkamp et al., 2004). The change in crystalline lens shape and alignment has implications for the accommodative mechanism and for accommodative optical performance. This thesis will present measurements of phakometry, tilt and decentration of the crystalline lens in the unaccommodated state (Chapters 2, 6, 9 and 10) and phakometry as function of accommodation (Chapter 5) in humans and phakometry and lens tilt and decentration as function of accommodation in rhesus monkeys (Chapter 7). Figure 1.5 shows biometric changes with accommodation in the human lens using Scheimpflug camera, and Figure 1.6 shows the tendencies in lens surface with accommodation obtained from Vilupuru and Glasser (Vilupuru & Glasser, 2003) and Glasser (Glasser et al., 2006) in rhesus monkeys.

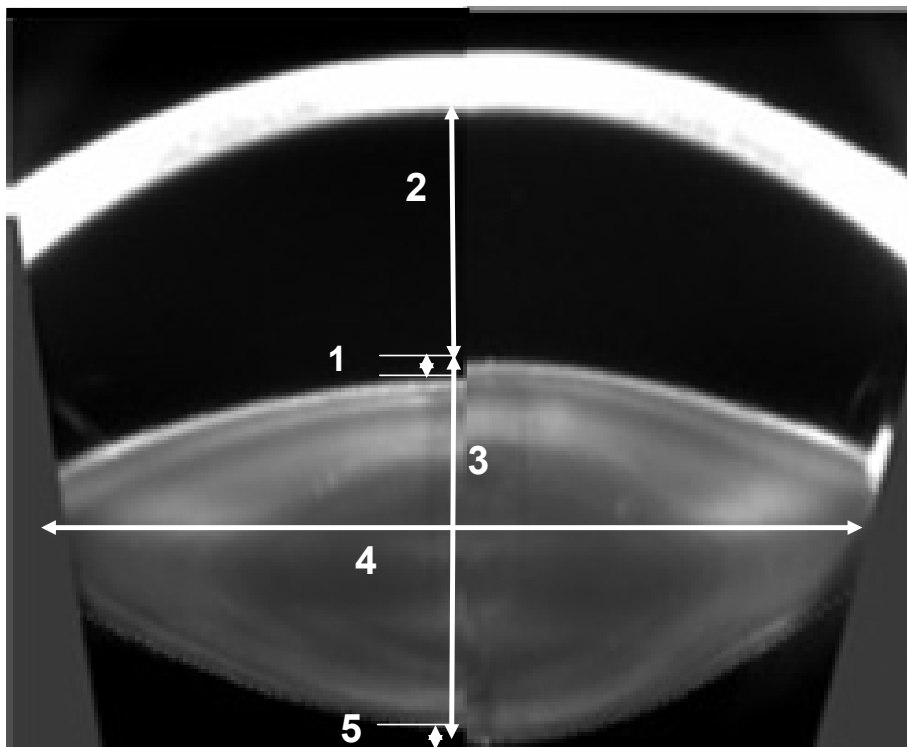


Figure 1.5. Illustration of the biometric changes with accommodation. The left half of the image corresponds to the unaccommodated state and the right half to the accommodated state. The changes indicated in the image include: 1. Forward movement of the anterior lens surface; 2. Decrease in anterior chamber depth. 3. Increase in lens thickness. 4. A. Decrease in lens equatorial diameter with increased accommodation and B. Centripetal ciliary processes (not indicated in the image). 5. Accommodative backward movement of the posterior lens surface. Courtesy of Rob van der Heijde and Michiel Dubbelman.

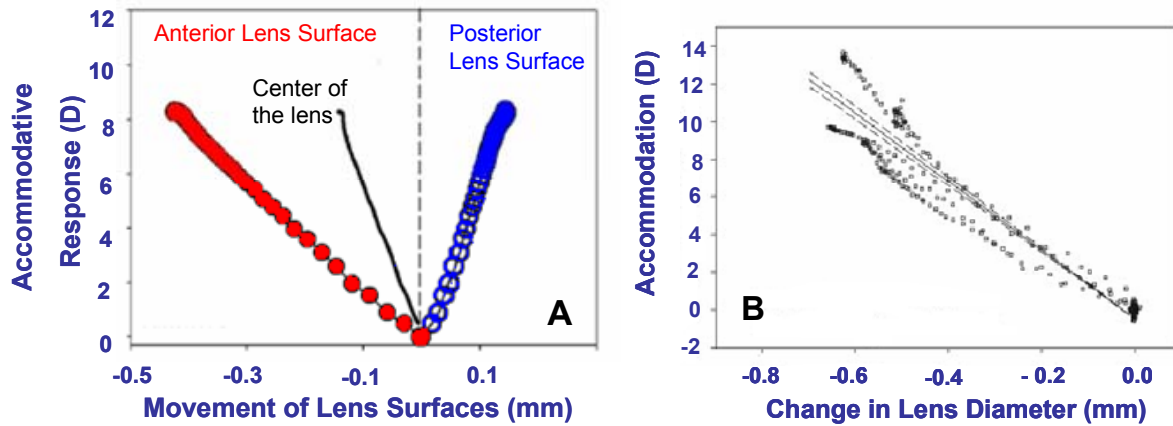


Figure 1.6. Crystalline lens biometric changes with accommodation. **A.** Represents the forward movement of the anterior lens and the backward movement of the posterior lens surface as the accommodative response increases. **B.** Represents the decrease in lens diameter with accommodation. The plots have been adapted from Vilupuru & Glasser (Vilupuru & Glasser, 2005).

2.3 The aging of the crystalline lens: presbyopia and cataracts

With increasing age, there are important optical and physical changes in the human crystalline lens. These changes are continuous through life, although their effects are more evident after the age of 40 years. The effect from which the eye loses its ability to accommodate affecting performance in near tasks is called presbyopia. The causes of presbyopia have been studied from physiological (Dubbelman et al., 2005, Glasser & Campbell, 1998, Glasser & Campbell, 1999, Kasthurirangan et al., 2007, Koretz et al., 2001, Koretz et al., 2002, Koretz et al., 1984, Koretz, Kaufman, Neider & Goeckner, 1989, Moffat, Atchison & Pope, 2002a, Strenk et al., 2004), anatomical (Croft et al., 2001, Glasser et al., 2001), biomechanical (Burd, Judge & Flavell, 1999, Hermans, Dubbelman, van der Heijde & Heethaar, 2006, Judge & Burd, 2002, Weeber & van der Heijde 2007), and biochemical approaches (McGinty & Truscott, 2006, Y Bron, Vrensen, Koretz, Maraini & Harding, 2000) although complete understanding is difficult due to the complexity of the process.

2.3.1 The aging lens

Several physical, biometric, optical and morphophysiological changes associated with aging of the human crystalline lens include (Agarwal, 2002, Croft et al., 2001, Glasser et al., 2001, Marcos, Barbero, McLellan & Burns, 2003):

Increased mass. Lens weight increases linearly from approximately 1100 mg at the end of the first year after birth to 200 mg at the age of 80 years, as has been shown from in vitro measurements of the excised lens (Smith, 1883, Willekens, Kappelhof & Vrensen, 1987).

Increased lens thickness. The crystalline lens thickness increases steadily with age after the age of 10 years (Zadnik, Mutti, Fusaro & Adams, 1995). Using in vivo Scheimpflug imaging, it has been shown that with age, the anterior lens surface moves toward the cornea, which results in a decrease of the anterior chamber depth of about 10 $\mu\text{m}/\text{year}$ (Dubbelman & van der Heijde, 2001, Koretz et al., 1989) and increase in lens thickness at a rate about of 24 $\mu\text{m}/\text{year}$ (Dubbelman et al., 2001) or 13 $\mu\text{m}/\text{year}$ (Koretz et al., 1989), depending upon whether the distortion correction applied to the Scheimpflug images or not.

Increased anterior and posterior surface curvatures. In vivo Scheimpflug measurements of unaccommodated eyes suggest that the lens anterior and posterior surface curvature increase with increasing age, although corrected Scheimpflug imaging (Dubbelman & van der Heijde, 2001) showed less extent in the increased lens curvatures than uncorrected ones (Brown, 1974, Koretz et al., 2001). These results have led to what has been described as the “lens paradox” (Koretz & Handelman, 1986b, Koretz & Handelman, 1988), since the curvature of the human eye lens increases (steepens) with age, yet most human eyes do not become more powerful as they get older (Moffat, Atchison & Pope, 2002b), changes in the index of refraction with age has been postulated.

Increasing lens curvatures should produce an optically more powerful lens and an eye focused for near vision. This thesis will provide validated measurements of anterior and posterior surface curvatures in human (Chapter 2, 6) and monkey eyes (Chapter 7).

Change in gradient refractive index. As an explanation of the “lens paradox”, it has been postulated that the lens gradient refractive index changes with increasing age to compensate for the increased surface curvatures. Empirical studies using calculations from population data suggest that the refractive index gradient does change to become relatively flatter in the nucleus of older lenses and that this could give a decrease in power of approximately 2D which matches the increased power due to increased thickness and surface curvatures (Hemenger et al., 1995, Ooi & Grosvenor, 1995). Other empirical studies have not been able to measure age-related changes of the index of refraction (Glasser & Campbell, 1999, Pierscionek, 1997). However, recent

measurements (Moffat et al., 2002a) of the gradient refractive index of excised lenses using magnetic resonance microimaging provides evidence for a change in the refractive index distribution as a function of age, which offsets the changes in lens curvature.

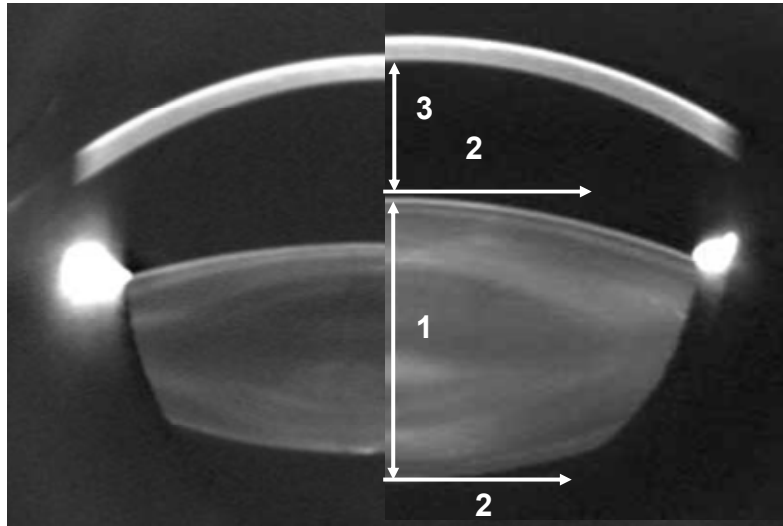


Figure 1.7. Illustration (using images from Scheimpflug photography) of the biometric changes with age in the crystalline lens. The left half of the image corresponds to a 16 years old crystalline lens, and right part of the image corresponds to a 54 years old crystalline lens. The changes indicated in the image include: 1 Increase lens thickness. Increase in refractive index. 2. Increase in anterior and posterior surfaces curvatures. 3. Anterior lens surface movement. Images provided by Dubbelman and van Der Heijde (Vrije University, Medical Center, Amsterdam).

Changes in the spherical aberration with age. Several methods have been used to measure the spherical aberration of the crystalline lens: 1) in vitro measurements of spherical aberration (along one meridian) of donor lenses, using a scanning laser apparatus (Sivak & Kreuzer, 1983), 2) neutralization of the cornea and measurement of the aberrations of the eye (Artal, Guirao, Berrio & Williams, 2001, Millodot & Sivak, 1979) and 3) measurement of total and anterior corneal aberrations and computation of the internal aberrations by subtraction of the two measurements (Artal & Guirao, 1998, El Hage & Berny, 1973). Glasser and Campbell (Glasser & Campbell, 1999) used the first method to assess the spherical aberration of the crystalline lens and found dramatic changes in the spherical aberration going from negative to positive with aging. Parallel beams were used in the experimental ray tracing rather than converging rays used in the other studies (for most distances, the cornea converges light from a target onto the lens), which prevents the measurements to be fully comparable. Artal (Artal, Berrio, Guirao &

Piers, 2002) used a subtraction method to estimate the aberrations of the crystalline lens as a function of age. They found an increase in the RMS of the aberrations of the crystalline lens with aging. Smith (Smith, Cox, Calver & Garner, 2001) measured the total and corneal spherical aberration and the crystalline lens by subtraction, in two group of young and old adults, and found lens spherical aberration to be less negative in the older group. The increase of spherical aberration with age found in the study by McLellan (McLellan et al., 2001) is also suggestive of an absolute increase of the spherical aberration of the crystalline lens. A more detailed review of optical aberrations will be addressed in Section 4 of this Chapter.

Morphophysiological changes with age. Several morphophysiological factors have been associated with the aging of the human crystalline lens, ciliary body, and zonular apparatus: 1) The capsule becomes thicker and less extensible with increasing age (Krag, Olsen & Andreassen, 1997). 2) Lens hardening (nuclear sclerosis), traditionally associated with decreased water content of the lens. Although the extent to which lens hardening occurs is debated, evidence has unequivocally demonstrated increased hardness of the lens with age (Fisher, 1971, Fisher, 1977, Glasser & Campbell, 1999).3) Aging of the ciliary muscle and zonules (Strenk, Semmlow & Strenk, 1999, Tamm, Tamm & Rohe, 1992). The zonular attachments are narrow, especially in the first two decades of life. The zonule-free zone of the anterior capsule reduces from 8 mm at age 20 years to 6.5 mm (or even as low as 5.5 mm) at about 80 years of age.

Figure 1.7 shows the changes with age in human crystalline lenses. The left side represents the young crystalline lens of a 16 years old woman, and the right side represents the eldest crystalline lens of her 54 years old mother. Figure 1.8 shows the tendencies with age for the anterior and posterior lens radius of curvature and anterior and posterior lens positions.

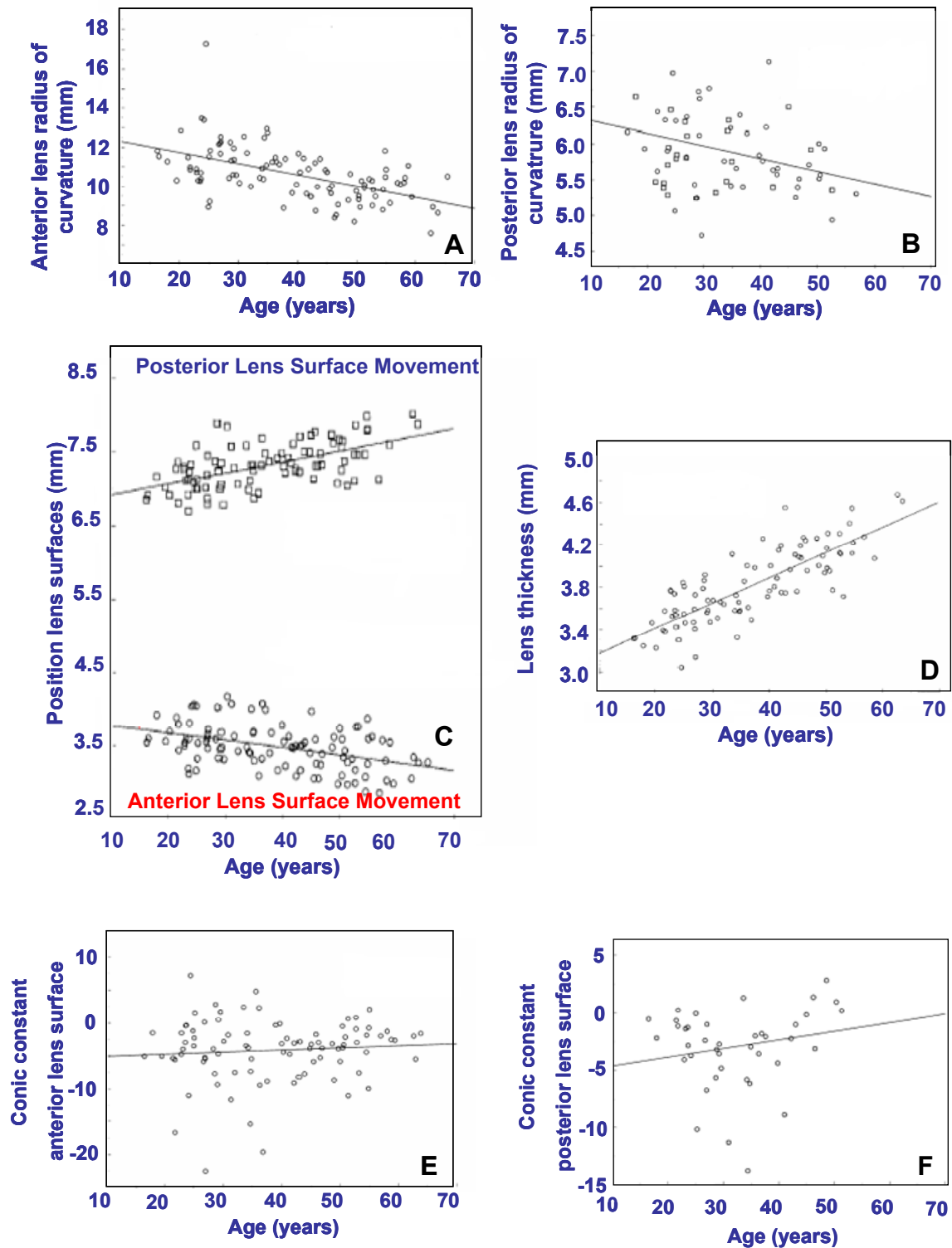


Figure 1.8. Crystalline lens biometric changes changes with age. **A.** and **B.** represent the changes in anterior and posterior lens radius of curvature with accommodation. **C.** represents the forward and backward movement of the anterior and posterior lens surfaces with accommodation. **D.** reflects the increase in lens thickness with accommodation. **E.** and **F.** plot the changes in anterior and posterior lens asphericity. Plots have been adapted from Dubbelman & van der Heijde (Dubbelman & van der Heijde, 2001).

3. IMAGING TECHNIQUES OF THE ANTERIOR SEGMENT OF THE EYE: AN OVERVIEW

The biometry and structural properties of the anterior segment of the eye (intraocular distances and shapes of the ocular components) can be assessed by various techniques. In this thesis we made use of several techniques to measure ocular biometry and structural properties of the cornea and crystalline lens, and implemented techniques for phakometry and measurement of lens misalignment. In this section we revise briefly the different techniques available, with a focus on a historical perspective. The techniques implemented in this thesis will be described in more detail in Chapters 2 and 3.

3.1. Techniques based on specular reflections from the ocular components.

3.1.1. Corneal videokeratometry

Corneal videokeratometry has been extensively used to obtain information of the shape of the anterior cornea (Campbell, 1997, Reynolds, 1980, Sicam & van der Heijde, 2006). The first corneal topograph can be dated to 1880, when the Portuguese ophthalmologist Antonio Placido viewed a painted disk (Placido's disk) of alternating black and white rings reflected in the cornea. The rings showed as contour lines projected on the corneal epithelium. In 1896, Allvar Gullstrand incorporated the disk in his ophthalmoscope, examining photographs of the cornea via a microscope and was able to manually calculate the curvature by means of a numerical algorithm. Gullstrand recognized the potential of the technique and commented it could "give a resultant accuracy that previously could not be obtained in any other way" (Gullstrand, 1909). The flat field of Placido's disk reduced the accuracy close to the corneal periphery and in the 1950s the Wesley-Jessen company made use of a curved bowl to reduce the field defects. The curvature of the cornea could be determined from comparison of photographs of the rings against standardized images.

In the 1980's, photographs of the projected images became hand-digitized and then analysed by computer. Automation of the process soon followed with the image captured by a digital camera and passed directly to a computer (Busin, Wilmanns & Spitznas, 1989). In the 1990s, systems became commercially available from a number of suppliers. In the corneal topographer used in this thesis (Humphrey-Zeiss MasterVue Atlas Model 990) the anterior corneal elevation was obtained using a Placido disk videokeratoscope which uses an arc step reconstruction algorithm. This system uses the

tear film as a convex mirror to view the first Purkinje image. The reflected image of the placido rings is captured on video camera and digitized. The computer analyses the position of each of the 15-38 circular mires along 256-360 semi-meridians, theoretically providing about 6,000 to 11,000 data points. Algorithms then compute the curvature at each point. The accuracy of measurements is about 0.15 D in the central zone of a normal cornea, but is commonly less in other situations due to the assumptions and approximations made by the algorithms. Corneal elevation maps are used in this thesis to generate computer eye models (Chapter 8), to compute corneal aberrations (Chapter 8 and 9). An extensive analysis of the accuracy of this corneal topography system and corneal aberrations estimation had been already performed in the Visual Optics and Biophotonics Lab at the Instituto de Optica, CSIC (Barbero, 2003, Barbero, Marcos, Merayo-Llolves & Moreno-Barriuso, 2002a, Barbero et al., 2002b).

3.1.2. Keratometry

A simpler method to obtain the anterior corneal radius of curvature is keratometry. A keratometer uses the first Purkinje image, PI, that is a reflection of a light source from the anterior cornea. The relationship between object size (O), generally multiple LED sources separated by a fixed distance; image size (PI), generally available on a camera; the distance between the reflective surface and the object (d), and the radius of curvature of the reflective surface (R) is given by the formula: $R = 2dPI/O$. In keratometry two meridians are measured, the steepest and the flattest. These measurements provide the anterior corneal radius of curvature, focusing power (assuming a particular refractive index for the cornea) and the amount of corneal astigmatism.

In this thesis, a keratometer to measure the apical corneal radius of curvature, was implemented to process phakometry data in a Rhesus Monkey model (Chapter 7).

3.1.3. Purkinje imaging phakometry

Purkinje images PIII and PIV are formed by reflections in the anterior and posterior crystalline surfaces and can be used to estimate the radii of curvature of the crystalline lens.

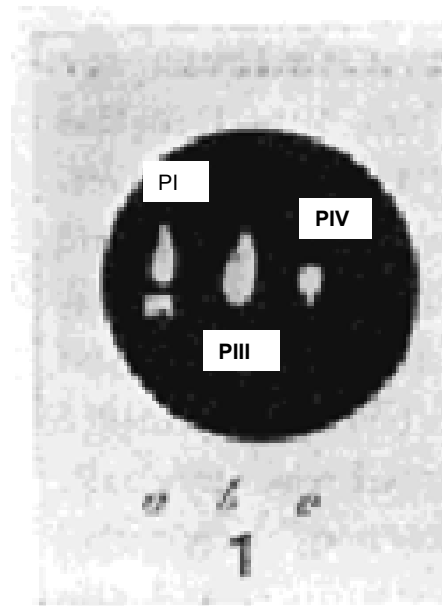


Figure 1.9. Original Purkinje images obtained by Purkinje. These are formed by reflections of a candle light by the different ocular surfaces. First Purkinje image comes from the anterior cornea, the third Purkinje image comes from the anterior lens surface and fourth Purkinje image comes from reflection of the posterior lens surface.

Since their description by Purkinje in 1832 (Figure 1.9) Purkinje images have been widely used to obtain the power of the crystalline lens, or the change of crystalline lens radii with accommodation. Several algorithms have been proposed to obtain anterior and posterior crystalline lens radii of curvature from Purkinje images. Smith and Garner (Smith & Garner, 1996) developed the so-called Equivalent Theorem Mirror method, based on the replacement of the different ocular surfaces by a single mirror. Garner (Garner, 1997) proposed the alternative recursive method called the merit function to obtain radii of curvature of the lens surfaces. This method was implemented experimentally by Barry and Dunne (Barry, Dunne & Kirschkamp, 2001) with physical model eyes and has been used to study the change of equivalent and gradient refractive index of the crystalline lens with accommodation (Garner & Smith, 1997), the changes in ocular dimensions and refraction with accommodation (Garner & Yap, 1997), and the refractive index of the crystalline lens in young and aged eyes (Garner et al., 1998). In this thesis we have developed a Purkinje-imaging based method to measure phakometry and tilt and decentration of the crystalline lens or intraocular lenses. A detailed description can be found in Chapter 2, and applications of it are given in Chapters 5, 6, 7, 9 and 10.

3.2. Ultrasound-based techniques

A widespread technique to measure intraocular distances (most commonly axial length, but also corneal thickness, anterior chamber depth and lens thickness) is ultrasound biometry (A-scan). The technique has also been developed to produce 3-D images of the anterior segment of the eye (ultrasound biomicroscopy). These are contact techniques, which are routinely performed under topical anesthesia.

3.2.1. A-scan Biometry

A-scan ultrasound biometry (Mundt & Hughes, 1956) relies on the generation of extremely high frequency sound waves that penetrate the eye and give a measurement of distances between the probe and specific structures. The sound wave is produced by a probe vibrating at a frequency of 10 MHz. The A-scan biometer pulses an electrical current to the tip of its probe, inducing a crystal to vibrate and emit the sound beam. The parallel sound beam travels from the point of contact (anterior surface of the cornea) through the eye. Several microseconds later, the A-scan pulse stops in order to detect echoes received from the reflection of the sound beam. These echoes are then converted to characteristic spikes and visualized on the biometer's display system. An echo bounces back to the probe tip whenever the beam encounters a media interface with different densities.

More recently, A-scan ultrasonography has been adapted to perform biometric changes dynamically. The so-called Continuous Ultrasound Biometry (CUB) (Beers & van der Heijde, 1994a, Vilupuru & Glasser, 2005), developed by van der Heijde and colleagues allows high-resolution A-scan biometric measurements at 100 Hz, using a 10-MHz transducer. The transducer contacts the cornea through ultrasound transmission gel to generate sharp A-scan peaks representing the anterior and posterior cornea surfaces, anterior and posterior lens surfaces, and the retina. The CUB measures the time between peaks associated with the intraocular surfaces. This method has proven to be a reliable and precise method to measure small, to about 1 μm , sagittal intraocular movements. This method has been used to measure microfluctuation in the lens and axial length during steady state accommodation (van der Heijde, Beers & Dubbelman, 1996), to model the dynamic behavior of the accommodation system (Beers & van der Heijde, 1994a, Beers & van der Heijde, 1994b, Niessen, De Jong & van der Heijde, 1992), to measure thickening and translation of the aging lens (van der Heijde,

Dubbelman & Beers, 1999), and it has been also extensively used in dynamic accommodation in monkeys (Vilupuru & Glasser, 2002, Vilupuru & Glasser, 2005). CUB is able to measure changes in the intraocular distances with a precision of 1 μm . This high precision should not be confused with the accuracy, which is limited by the wavelength of the ultrasonic pulse, i.e. approximately 0.15 mm. In this thesis, this technology has been used to assess dynamic changes of anterior chamber depth and lens thickness in monkeys and to process dynamic phakometry data in Chapter 6.

3.2.2 Ultrasound biomicroscopy

While in A-scan ultrasonography, a thin, parallel sound beam is emitted, which passes through the eye and images one small axis of tissue; the echoes of which are represented as spikes arising from the baseline, in B-scan ultrasonography an oscillating sound beam is emitted, passing through the eye and imaging a slice of tissue; the echoes of which are represented as a multitude of A-scan which can be combined to generate an image.

Three-dimensional (3-D) ultrasound is the natural extension of two-dimensional B-scan imaging (Coleman, Woods, Rondeau & Silverman, 1992, Downey, Nicolle, Levin & Fenster, 1996, Jensen & Hansen, 1991, Jazzi, Rosen & Tello, 1996, Silverman, Rondeau, Lizzi & Coleman, 1995). The 3-D image is constructed from ultrasound data acquired in a series of ordered B-scan planes that are either parallel to each other or separated by regular angular increments. The 3-D ultrasound allows evaluation of hidden ocular structures and measurement and monitoring of the shape and volume of normal and pathologic ocular structures. Ultrasonography performed at standard frequencies (10 MHz), providing a resolution of approximately 150 μm , is insufficient to resolve fine details of ocular structures, or assess complex surface shapes. The use of improved transducer technology (Pavlin, Harasiewicz, Sherar & Foster, 1991, Pavlin, Sherar & Foster, 1990) allowed very high ophthalmic ultrasound scanning frequencies (VHF) in the 30- to 80 MHz range in a commercial instrument, the Ultrasound Biomicroscope (Humphrey Instruments, San Leandro, CA). These higher frequencies, although limited in application to the anterior segment, provide a resolution of approximately 35 μm . Commercial ultrasound scanning systems using intermediate frequency ranges (15-30 MHz) or interchangeable transducers permitting scanning at various frequency ranges have also been introduced (Cusumano, Coleman, Silverman, Reinstein, Rondeau, Ursea, Daly & Lloyd, 1998). The system incorporates two

computer-controlled linear motion stages mounted at right angles to each other. By moving the transducer in a series of parallel planes, a sequence of VHF ultrasound images suitable for 3-D reconstruction of the anterior segment can be acquired. Recent developments involve digitization of radio frequency (RF) ultrasound data, rather than the processed envelope of the data (which discards phase information with consequent reduction in measurement accuracy). From ultrasonic RF data, spectrum analysis can be performed using frequency-domain signal processing techniques (Allemann, Silverman, Reinstein & Coleman, 1993, Reinstein, Silverman, Trokel & Coleman, 1994, Silverman et al., 1995). Spectrum analysis can provide quantitative information on the structure of tissue inhomogeneities smaller than those directly resolvable on conventional B-scan images.

3.3. Techniques based on low coherence interferometry

3.3.1. Partial coherence interferometry

In general, A-scan biometry is easy to perform and gives accurate results in the majority of patients. However, the most commonly performed type of ultrasound A-scan (applanation biometry) requires contact with the cornea, and the force applied on the cornea does decrease the measured axial length by a fraction of a millimeter. Advances in partial coherence interferometry now allow a non-contact way of measuring interocular distances. This technique relies on optical interferometry rather than ultrasound. A superluminescent diode in a Michelson interferometer emits a 780 nm infrared light with short coherence length light to determine the distance from the cornea to the retinal pigment epithelium. Drexler et al. were the first to describe the partial coherence interferometry (Drexler, Baumgartner, Findl, Hitzenberger, Sattmann & Fercher, 1997, Drexler, Findl, Menapace, Rainer, Vass, Hitzenberger & Fercher, 1998), and also suggested, a special heterodyne detection technique, called laser Doppler interferometry (Drexler, Hitzenberger, Sattmann & Fercher, 1995, Hitzenberger, 1991) to obtain short measurement times. This technique has been used for anterior chamber depth (Kriechbaum, Findl, Kiss, Sacu, Petternel & Drexler, 2003, Kriechbaum, Findl, Preussner, Koppl, Wahl & Drexler, 2003), corneal thickness (Rainer, Petternel, Findl, Schmetterer, Skorpik, Luksch & Drexler, 2002) and axial length measurements, and subsequently used to calculate more accurately intraocular

lens power (Findl, Drexler, Menapace, Heinzl, Hitzenberger & Fercher, 2001, Rajan, Keilhorn & Bell, 2002) .

In this thesis we used a commercially available apparatus (IOL Master, Zeiss Humphrey), based on partial coherence interferometry to obtain biometric measurements for phakometry/IOL tilt and decentration measurements in Chapters 2, 5, 8 and 9. The disadvantage of the commercial instrument is that only axial length measurements are based on interferometry, while anterior chamber depth measurements are based on slit-lamp imaging. In addition it does not allow continuous optical biometric measurements during accommodation.

3.3.2 Optical Coherence Tomography (OCT)

First devised in 1991 by Huang (Huang, Swanson, Lin, Schuman, Stinson, Chang, Hee, Flotte, Gregory & Pulifito, 1991, Li, Shekhar & Huang, 2006) and Fercher (Fercher, Hitzenberger, Drexler, Kamp & Sattmann, 1993) in 1993 and later improved by Izatt (Izatt, Hee, Swanson, Lin, Huang, Schuman, Puliafito & Fujimoto, 1994) in 1994 for anterior chamber imaging, optical coherence tomography (OCT) with micrometer resolution and cross-sectional imaging capabilities, has become a prominent biomedical tissue imaging technique. With this technique it is possible to perform non-invasive cross-sectional imaging of internal structures in biological tissues by measuring their optical reflections.

Optical Coherence Tomography (OCT) (Huang, Swanson, Lin, Schuman, Stinson, Chang, Hee, Flotte, Gegory, Puliafito & Fujimoto, 1991) has found widespread applications for cross sectional imaging of tissue *in situ* with micron scale resolution. Earlier OCT systems were based on time domain detection where echo time delays of light were detected by measuring the interference signal as a function of time, while scanning the optical path length of the reference arm (Drexler, Morgner, Kartner, Pitris, Boppart, Li, Ippen & Fujimoto, 1999, Swanson, Huang, Hee, Fujimoto, Lin & Puliafito, 1992). Recently, OCT techniques based on Fourier domain detection have become an active area of research (Fercher, Hitzenberger, Kamp & Elzaiat, 1995, Park, Pierce, Cense, Yun, Mujat, Tearney, Bouma & de Boer, 2005). OCT with Fourier domain detection uses either a spectrograph (Fercher et al., 1995, Häusler & Lindner, 1998) or a frequency swept laser source (Chinn, Swanson & Fujimoto, 1997, Choma, Hsu & Izatt, 2005, Fercher et al., 1995, Yun, Tearney, De Boer, Iftimia & Bournia, 2003) to measure echo time delays of light by spectrally resolving the interference signal. The magnitude

and time delay of the backscattered light is reconstructed by Fourier transformation of the fringe signal versus frequency. Recent studies have shown that Fourier domain detection using spectrometers or frequency swept lasers can dramatically improve the detection sensitivity and enable significantly higher scan speeds than standard time domain detection techniques (Choma, Sarunic, Yang & Izatt, 2003, de Boer, Cense, Park, Pierce, Tearney & Bouma, 2003). Time domain OCT imaging using two-dimensional zone focusing and image fusion or focus tracking to increase the depth of view has been demonstrated, but suffers from slow data acquisition speeds (Cobb, Liu & Li, 2005, Drexler et al., 1999, Lexer, Hitzenger, Drexler, Molebny, Sattmann, Sticker & Fercher, 1999). Full, three-dimensional data sets with enhanced depth of field can be acquired within several seconds by acquiring and fusing multiple three dimensional data sets with different focus depths. This overcomes depth of field limitations which are normally associated with the small focused spot sizes required for high transverse resolution.

Anterior segment OCT systems are less common than retinal systems. Commercial systems have been recently introduced, but these tend to provide more qualitative than quantitative information of geometrical parameters. Izatt (Goldsmith, Li, Chalita, Westphal, Patil, Rollins, Izatt & Huang, 2005) in 2005 proposed a novel high-speed (4000 axial scans/second) OCT prototype anterior segment scanning that used a long wavelength (1310 nm) for deeper angle penetration, rectangular scanning for undistorted imaging, and short image acquisition time (0.125 seconds) to reduce motion error to obtain three horizontal cross-sectional OCT images (15.5 mm wide and 6 mm deep) of the anterior segment .

3.4. Magnetic Resonance Imaging (MRI)

Magnetic resonance imaging (MRI) is an imaging technique used primarily in medical settings to produce high quality images of the inside of the human body. MRI is based on the principles of nuclear magnetic resonance (NMR), a spectroscopic technique used by scientists to obtain microscopic chemical and physical information about molecules. MRI started out as a tomographic imaging technique and has advanced to a volume imaging technique. This technique is capable of producing undistorted images of the whole eye in vivo and has been used to study the anterior segment of the aging eye by Strenk (Strenk et al., 2005, Strenk et al., 2004, Strenk et al., 1999, Strenk & Strenk, 2006). However, up until now, the disadvantage of this method is the poor

resolution of the images of ± 0.2 mm. Therefore, the method is not appropriate to measure small changes and the asphericity of the surfaces.

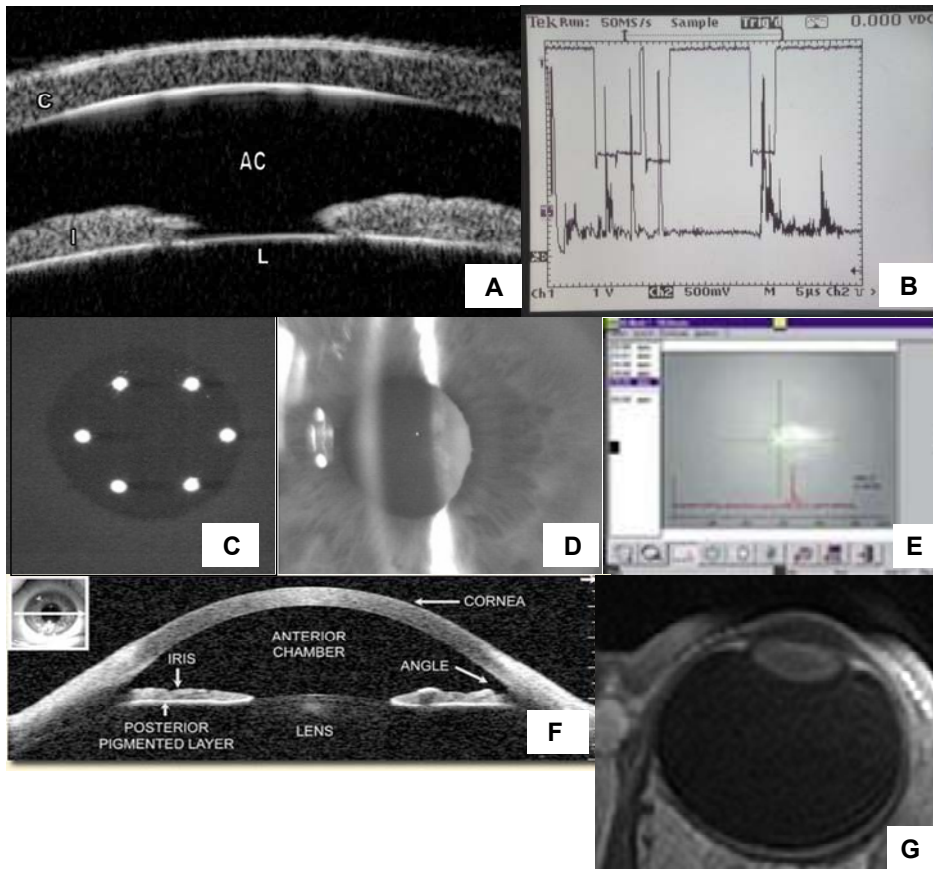


Figure 1.10. Illustration of image outputs from several anterior segment imaging/ocular biometry techniques: **A.** Ultrasound biomicroscopy (adapted from de Guzman et al. 2005)(de Guzman, Thiagalingam, Ong & Goldberg, 2005); **B.** A-Scan from Continuous Ultrasound Biometry (Courtesy of Rob van der Heijde). **C.** Keratometry **D.** Anterior chamber depth from slit lamp imaging **E.** Partial coherence interferometry for axial length measurements (c) with the IOLMaster (Zeiss). **F.** Anterior chamber image obtained with Optical Coherence Tomography (Adapted from the New York Eye Enfermery) **G.** Image of the eye globe obtained by Magnetic Resonance Imaging (Adapted from Strenk et al. 2004)

3.5. Slit lamp biomicroscopy

In this system, invented by Alvar Gullstrand in 1911, a narrow "slit" beam of very bright light produced by a lamp is focused on to the eye which is then viewed under magnification with a microscope (Gullstrand, 1911). The illumination system is composed by a light source and condensing lenses which allow uniform illumination of a slit aperture (with generally variable width, length and orientation). Magnification of the observing microscope ranges from about x 10 to about x 50. While this technique is extremely useful for clinical examinations, it is limited to provide quantitative information of ocular component dimensions by small depth of focus, that prevents

obtaining a sharp image of the cornea and the lens simultaneously. Figure 1.11 shows the principle of Slit-Lamp photography.

3.5.1 Scanning slit corneal topography

The basis of the method is to photograph a series of slit-beam sections through the eye at varying angles to the optic axis (generally using a scanning optical slit device), to obtain an image of the profile of the anterior and posterior cornea (and in principle, also the lens, at least the anterior surface). Because of the refraction of the previous ocular surfaces, the shapes of the inner surfaces of the anterior segment imaged are distorted. Several studies have tested the validity of measurements of posterior corneal surface with the commercially available slit scanner, Orbscan (Maldonado, Nieto, Díez-Cuenca & Piñero, 2006, Quisling, Sjoberg, Zimmerman, Goins & Sutphin, 2006), but because a correction of optical distortion has not been reported, the accuracy of those measurements, is still unclear (Wilson, 2000).

3.5.2. Scheimpflug imaging

To obtain complete anterior segment images, the Scheimpflug imaging improves the slit lamp geometry, by using the Scheimpflug's principle. Normally, the lens and image (film or sensor) planes of a camera are parallel, and the plane of focus is parallel to the lens and image planes. If a planar subject (such as the side of a building) is also parallel to the image plane, it can coincide with the plane of focus, and the entire subject can be rendered sharply. If the subject plane is not parallel to the image plane, it will be in focus only along a line where it intersects the plane of focus, as illustrated in Figure 1.11 A. When an oblique tangent is extended from the image plane, and another is extended from the lens plane, they meet at a point through which the plane of focus also passes, as illustrated in Figure 1.11 B. With this condition, a planar subject that is not parallel to the image plane can be completely in focus.

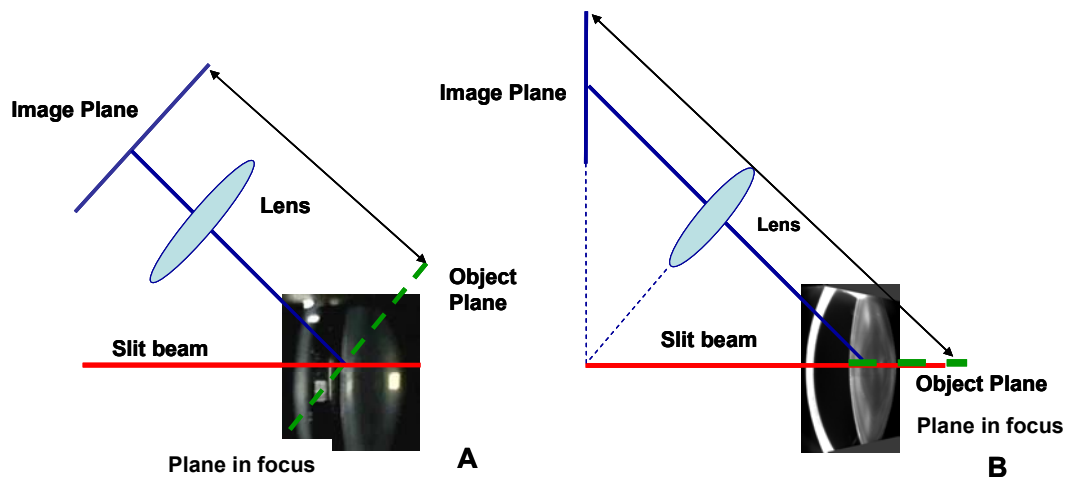


Figure 1.11. **A.** Principle of Slit lamp imaging. A slit beam is focused on the eye which is viewed with a microscope. The Plane image and Object image are parallel to each other. **B.** Principle of Scheimpflug imaging, where the image and objects planes are tilted with respect to each other in such way that they intersect in one point.

The special geometry of the Scheimpflug configuration allows imaging the anterior segment with large depth of focus, but it introduces a geometrical distortion, because the magnification is not constant over the image. Additionally, because of the refraction from the different ocular surfaces, the Scheimpflug camera also introduces an optical distortion, due to the fact that each of the ocular surfaces is seen through the previous one (i.e., the anterior lens is seen through the posterior and anterior cornea). In order to obtain reliable information from those images, those distortions must be corrected. The methods for correction of these distortions are further explained in Chapter 3. In this thesis two different Scheimpflug instruments have been used and evaluated. A modified Topcon SL-45 corrected system (Chapter 4) for phakometry. A Pentacam (Oculus) system in Chapter 5 for intraocular lens tilt and decentration measurements.

4. THE OPTICAL QUALITY OF THE NORMAL HUMAN EYE

The eye is an optical instrument that projects scenes of the visual world onto the retina. It has been known for many years that the eye is far from being a perfect optical system, in particular for large pupil diameters. Refractive anomalies (defocus or astigmatism) occur frequently in the eye.

However the eye suffers also from other optical imperfections (called high order aberrations). Like defocus, optical aberrations blur the retinal image, reducing image

contrast and limiting the range of spatial frequencies available to further stages of the visual processing. With the development of rapid and reliable aberrometers, ocular aberrations can be easily measured. The contribution of the cornea to the overall aberrations of the eye can be also be computed from corneal topography. The contribution of the internal optics to the ocular aberration of the eye is typically estimated by subtracting corneal from total aberrations. However, the sources of optical aberrations in the crystalline lens, and misalignments of the optical components are not well understood. This thesis will shed light into the contributions of lens shapes and misalignments to the optical degradation in the normal eye, and most completely the pseudophakic eye.

4.1 Optical aberrations.

The wave aberration, $W(x, y)$, defines how the phase of light is affected as it passes through the optical system. The wavefront is a line that joins every point on a wave that has the same phase, i.e it is a surface that joins the leading edges of all rays at some instant. The wave aberration is defined as the deviation of this wavefront from a reference surface that is usually defined as a surface of curvature near the wavefront whose origin is located at the Gaussian image point (where the light would be focused if the eye were perfect) (Figure 1.12). If the Gaussian image is at infinity, then it follows that the reference surface is a plane. For the human eye, the natural choices for the reference would be a sphere whose center of curvature is at the fovea for line-of sight (Applegate, Thibos, Bradley, Marcos, Roorda, Salmon & Atchison, 2000) measurements, or at infinity for light emerging from the eye.

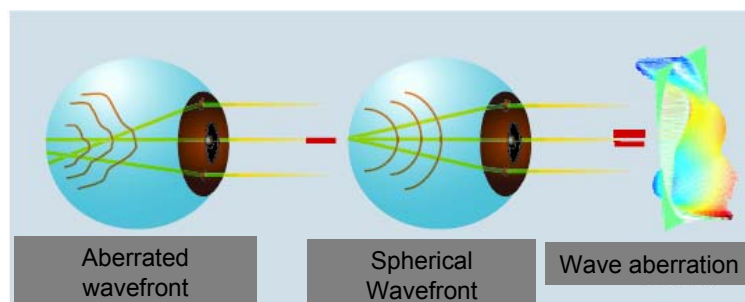


Figure 1.12. Schematic diagram of the concept of ocular wavefront aberration **A**. The wave front takes a spherical shape for a diffraction-limited optical system **B**. The wave front of an aberrated optical system is irregular, wave front aberration WA is defined as the deviation of the wave front from a reference wave front. Figure adapted from Marcos (Marcos, 2005)

The wave aberration is often defined mathematically by a series of polynomials, such as the Seidel polynomials, but these can define only a limited range of aberrations. Howland (Howland & Howland, 1977) proposed a Taylor expansion to describe the wave aberration function in terms of pupil coordinates. The most popular polynomials are Zernike polynomials, first introduced by Frits Zernike in interferometric contrast phase microscopy (Zernike, 1934). The main advantage of the set of Zernike polynomials is that they are orthonormal in a unit circle. As pupil coordinates are usually normalized for a unit circle, any continuous wave aberration function can be expressed in terms of a Zernike expansion. Each Zernike term is formed by the product of a radial, an angular function and a normalization factor, specified by radial indexes. The Optical Society of America has established a set of recommendations (Thibos et al., 2000) about sign, normalization (Noll's normalization) and ordering, that has been followed in this thesis. Figure 1.13 shows the representation of the Zernike polynomial terms from 2nd to 4th order polynomials.

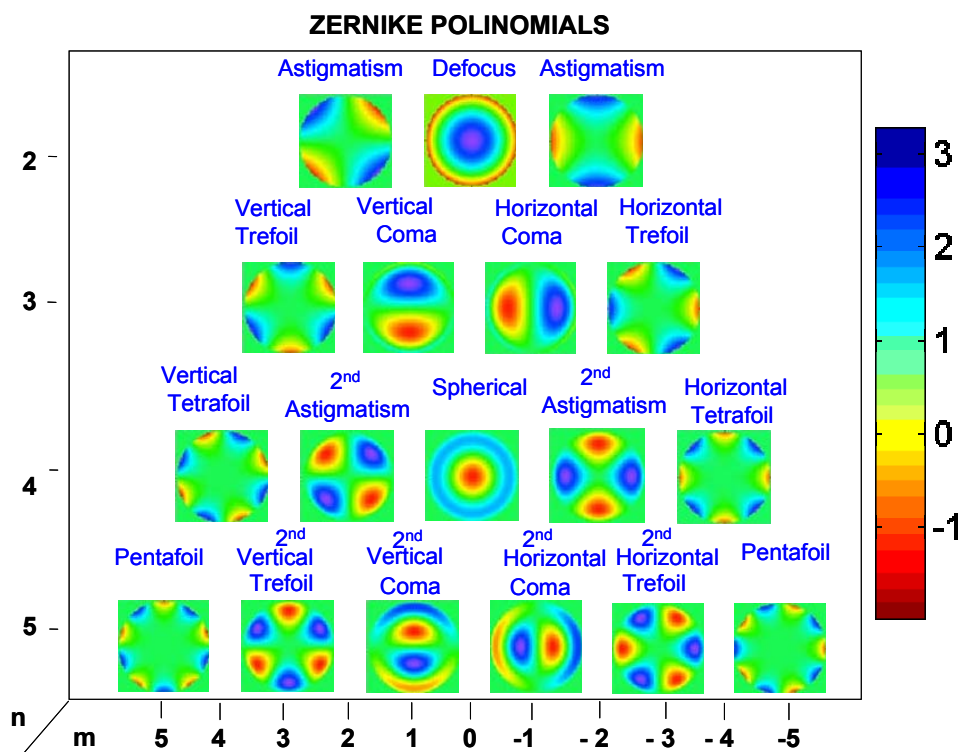


Figure 1.13. Representation of the Zernike polynomial terms from 2nd to 4th order polynomials, according to the Optical Society of America nomenclature (Thibos, Applegate, Schwiegerling, Webb & Members, 2000). The scale is in microns.

4.2 Aberrometry

Many scientists throughout the history of physiological optics have attempted to measure the optical aberrations of the human eye. Scheiner in 1619 (Scheiner, 1619) published the work "Oculus, sive fundamentum opticum" where he announced the invention of a disc with a centered and a peripheral pinhole that was placed before the eyes of a subject to view a distant light source. If the subject saw a single spot he was an emmetrope, if he saw two inverted spots, he was a myope; and if he saw two upright spots, a hyperope. This device was the first qualitative refractor and became known as Scheiner's disc. After Scheiner, many scientists attempted to construct more precise refractors. Tscherning (Tscherning, 1894) in 1894 used a four-dimensional spherical lens with a grid pattern on its surface to project a regular pattern on the retina. He would then ask the patient to sketch drawings of the pattern. Depending on the pattern's distortion, Tscherning was able to obtain a semiquantitative measurement of the patient's aberrations. One of the earliest quantitative aberrometers was devised by Howland (Howland, 1960, Howland & Howland, 1976, Howland & Howland, 1977). The aberroscope consisted of a nearly square grid mounted between the plane surfaces of +5 and -5 D plano-cylindrical lenses, with the cylindrical axes mutually perpendicular and at 45 deg to the vertical. The grid is distorted slightly so that it projects squares onto the entrance pupil of the eye. A shadow of the grid is formed on a subject's retina. The initial version of this technique was subjective. Howland and Howland analyzed sketches of grid shadows drawn by their subjects to obtain wave-aberration polynomials and optical transfer functions. Walsh (Walsh, Charman & Howland, 1984) and Walsh and Charman (Walsh & Charman, 1985) made the technique objective by inserting a beam splitter between the aberroscope and the eye, so that the retinal grid shadow could be photographed.

Another subjective technique first introduced by Smirnov (Smirnov, 1961) for testing the human eye by spatially examining the refractive performance of light rays point by point across the entire pupil was not widely adopted in the study of aberrations of the eye because it was time consuming. A faster implementation of Smirnov's technique was developed by Webb (Webb, Penney & Thompson, 1992), and called the spatially resolved refractometer (SRR). A new version of the SRR was developed by He (He, Marcos, Webb & Burns, 1998) that allows rapid estimates of both the overall wave-front aberration and individual aberrations. An objective version of the SRR, the

Laser Ray Tracing (LRT) technique was developed by Navarro and Moreno-Barriuso (Navarro & Moreno-Barriuso, 1999). The method consists of delivering narrow pencils of light (rays) sequentially through the optical system and measuring the position (centroid) of the image spot on the detector (image) plane. It is possible to scan the pupil plane by sequentially delivering rays through different pupil positions. A new generation of a much more compact LRT system was developed, with significant improvements over the first generation (Llorente et al., 2004). This system is used in the current thesis in Chapters 8 and 9, and will be briefly described in Chapter 8.

Figure 1.14 shows the laser ray tracing set up used to measure the ocular aberrations reported in this thesis. Briefly, the light source is either a green (532 nm) or infrared (786 nm) laser diode. An x-y scanner deflects the rays. The light reflected back from the retina is captured by high-resolution camera CCD₂ conjugate to the retina. Another camera (CCD₁) conjugate to the pupil and coaxial with the system captures images of the pupil simultaneously and is used for continuous alignment.

One of the most popular aberrometric techniques is the so-called Hartmann-Shack wavefront sensor. Liang (Liang, Grimm, Goelz & Bille, 1994) applied to the human eye an idea originally applied to general optical instruments such as astronomical telescopes since the 1950s (Babcock, 1953). The sensor used to measure the aberrations was first developed by Hartmann in 1900 (Hartmann, 1900) and later improved by Shack in 1971 (Shack & Platt, 1971). This sensor became known as the Hartmann-Shack sensor, abbreviated HS sensor, which consists of a mono-lithic array of small circular apertures (microlenses) to sample the wave front in a reference sphere at the exit pupil, as opposed to the LRT which uses a single Gaussian beam as a ray whose coordinates (for both the point object and the entrance-pupil position) can be specified as in standard ray-tracing software. Studies at the Visual Optics and Biophotonics laboratory have shown the equivalency of LRT, HS and SRR on human eyes (Llorente, Diaz-Santana, Lara-Saucedo & Marcos, 2003, Marcos, Díaz-Santana, Llorente & C., 2002, Moreno-Barriuso, Marcos, Navarro & Burns, 2001).

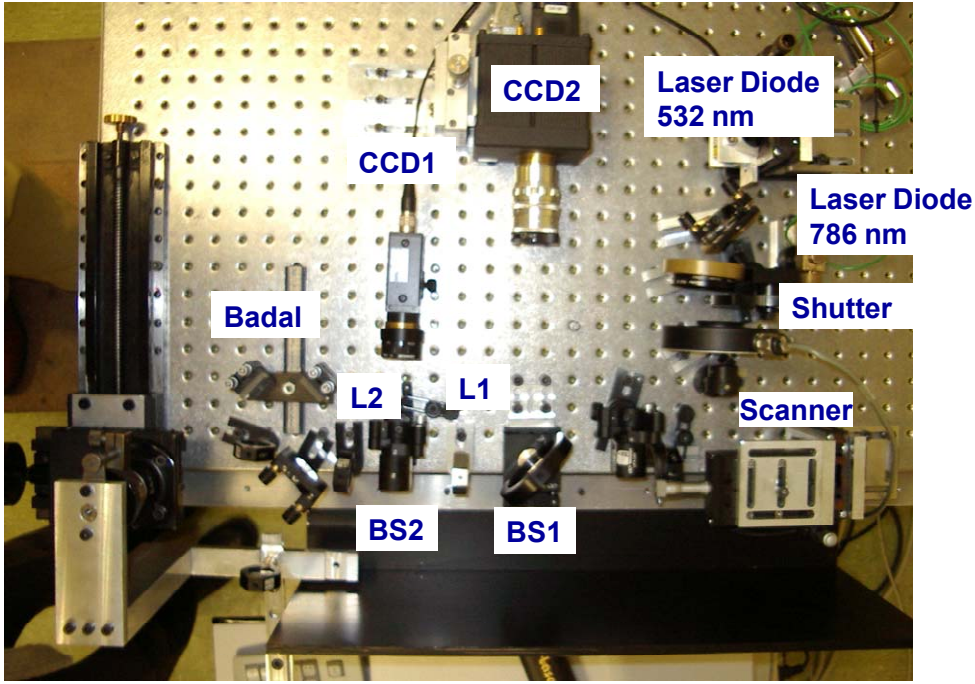


Figure 1.14. Photograph of the Laser Ray Tracing set up at the Visual Optics and Biophotonics Lab (Instituto de Optica). A detailed description of the principle and technical specifications of the system appear in the text. This system, developed previous to this thesis, has been used to measure the ocular aberrations reported in this thesis.

The principle for wave front measurements can be summarized as follows.

Considering a mathematical expression of the wave aberrations in terms of Zernike polynomials:

$$W(x, y) \approx \sum_{m=1}^{37} Z_m P_m(x, y) \quad [1.1]$$

with Z_m being the coefficients of the expansion, in microns, and P_m the Zernike polynomials.

The eye's pupil is sampled at a set of points (X_i, Y_i) $i = 1, \dots, n$ according to a sampling pattern. Normalizing the pupil coordinates, given by $\bar{X} = \frac{X}{R_p}$ and $\bar{Y} = \frac{Y}{R_p}$, (with R_p being the pupil radius), the ray aberrations $[\Delta x'(X_i, Y_i), \Delta y'(X_i, Y_i)]$

corresponding to the pupil locations can be obtained from the partial derivatives of the Wave Aberration (W):

$$\Delta x' = \frac{1}{R_p} \frac{\partial W(X, Y)}{\partial X}; \quad \Delta y' = \frac{1}{R_p} \frac{\partial W(X, Y)}{\partial Y} \quad [1.2]$$

The partial derivatives can be obtained from Equation [1.1], and the wave aberration can be obtained by least squares fitting of the ray aberration to the partial derivatives of the Zernike polynomials for each pupil location sampled.

4.3 Total aberrations

The amount and distribution of aberrations vary greatly among the population. Several population studies show a wide distribution of the aberrations in human eyes. Typically all high order terms average to zero. Smirnov (Smirnov, 1961) was the first to study the intersubject variability in the eye's wave aberration for a population of ten subjects. Howland and Howland (Howland & Howland, 1977) studied the monochromatic aberrations by using the aberroscopic technique and found that the wave aberration differs greatly across subjects. In particular, Porter (Porter, Guirao, Cox & Williams, 2001), Thibos (Thibos, Hong, Bradley & Cheng, 2002), Castejon Mochon (Castejon-Mochon et al., 2002) found that most of the total RMS were in the first two and three orders. They found a relative symmetry between aberration pattern between right and left eyes, although previous studies by Marcos & Burns (Marcos & Burns, 2000) and Castejon-Mochon reported some symmetry, but to a lesser extent.

Porter found that spherical aberration was the only mode to have a mean that is significantly different from zero, with a mean value of $0.138 \pm 0.13 \mu\text{m}$ for a 5.7 mm pupil. They found that even though there appears to be a random variation in the eye's aberrations from subject to subject, many aberrations in the left eye were found to be significantly correlated with their counterparts in the right eye. Other studies reported a negative mean significant value for oblique trefoil (Cheng, Barnett, Vilupuru, Marsack, Kasthurirangan, Applegate & Roorda, 2004, Thibos et al., 2002, Wang & Koch, 2003).

A recent review by Salmon (Salmon & van de Pol, 2006) combining Hartmann-Shack aberrometry data from multiple sites (a total of 2560 eyes from 1433 subjects) found that the most prominent modes were Z_3^{-3} (horizontal trefoil), Z_3^{-1} (vertical

coma), and Z_4^0 (spherical aberration), with mean absolute values of 0.11 μm , 0.14 μm , and 0.13 μm and average total higher-order RMS values (from the third to sixth order) of 0.33 μm for a 6 mm pupil.

4.4 Corneal Aberrations

Basic data regarding corneal wavefront aberrations, such as the distribution in the population and changes with aging, are essential to understanding the contribution of the cornea to the overall optical degradation. In young eyes the anterior cornea is typically steeper in the vertical than in the horizontal meridian, which results in corneal astigmatism. Interestingly this asymmetry tends to reverse with increasing age (Hayashi, Hayashi & Hayashi, 1995 i.e, corneal astigmatism changes from “with-the-rule” to “against-the-rule” with age). In general, the cornea becomes steeper with age.

Oshika (Oshika, Klyce, Applegate & Howland, 1999) estimated corneal aberrations from corneal elevation maps, finding that for a 7.0 mm pupil, total wavefront aberrations and coma-like aberrations of the cornea correlated with age, whereas spherical-like aberrations did not vary significantly with age. Because comalike aberrations consist of tilt and/or asymmetry, these results imply that the corneas become less symmetric with aging.

Guirao (Guirao, Redondo & Artal, 2000), using similar technique, reported that despite a large intersubject variability, the average amount of aberration of the human cornea tends to increase moderately with age, finding that spherical aberration was significantly larger in the middle aged (40-50 years old) and older corneas (60-70 years old).

Wang Li (Wang, Dai, Koch & Nathoo, 2003), studied corneal high order aberrations from the central 6.0 mm zone of the corneal topographic of mean age 50 years and found a wide individual variability in aberrations, with ranges of individual Zernike terms from -0.579 to +0.572 μm . The mean coefficient of the fourth order spherical aberration (Z_{40}) was $0.280 \pm 0.086 \mu\text{m}$ and positive in all corneas. The mean root-mean-square (RMS) values were $0.479 \pm 0.124 \mu\text{m}$ for high order aberrations, $0.281 \pm 0.086 \mu\text{m}$ for spherical aberration (Z_{40} and Z_{60}), and $0.248 \pm 0.135 \mu\text{m}$ for coma (Z_{3-1} , Z_{31} , Z_{5-1} , and Z_{51}). Moderate correlations were found between right and left eyes for high order aberration, spherical aberration, and coma. This study also reported an increase in high

order aberrations and coma with age, but spherical aberration did not show any dependence with age.

Using a distortion-corrected Scheimpflug camera, it has been found, that the posterior corneal surface compensates for 31% of the anterior corneal surface astigmatism, which is larger than could be expected based on the astigmatism of the anterior surface alone (Dubbelman, Sicam & van der Heijde, 2006). Scheimpflug studies also show that the spherical aberration of the posterior corneal surface (Sicam, Dubbelman & van der Heijde 2006) is negative at a young age and becomes positive at an older age, with the ratio (posterior spherical aberration)/(anterior spherical aberration) therefore shifting to compensate the positive spherical aberration of the cornea (-10%) in young subjects to add up aberration (26%) in old subjects. As for coma, these studies show the posterior corneal surface compensates approximately 3.5% the anterior surface coma, this compensation being larger for young subjects (6%) than for older subjects (0%). It can be therefore concluded that the posterior cornea has in general a small effect on high order aberrations of the eye, and that the slight compensation found in young eyes is lost with age (Dubbelman, Sicam & van der Heijde, 2007).

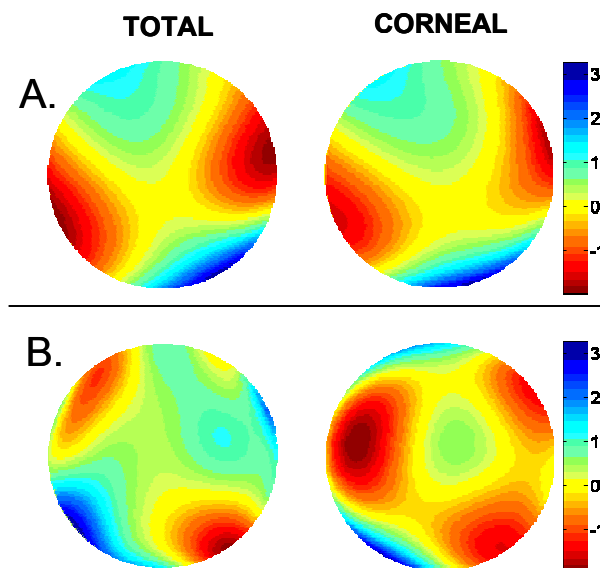


Figure 1.15. Total and corneal wave aberrations of both eyes of an unilateral aphakic 30-old patient. **A.** Aphakic eye (with no crystalline lens) and **B.** Normal contralateral eye. Note the similarity of corneal and total aberrations in the aphakic eye, and the compensation of corneal spherical aberration by the internal optics in the normal eye. Pupil diameter=6.5 mm. Figure adapted from Barbero (Barbero, Marcos & Merayo-Llodes, 2002b).

order aberrations and coma with age, but spherical aberration did not show any dependence with age.

Using a distortion-corrected Scheimpflug camera, it has been found, that the posterior corneal surface compensates for 31% of the anterior corneal surface astigmatism, which is larger than could be expected based on the astigmatism of the anterior surface alone (Dubbelman, Sicam & van der Heijde, 2006). Scheimpflug studies also show that the spherical aberration of the posterior corneal surface (Sicam, Dubbelman & van der Heijde 2006) is negative at a young age and becomes positive at an older age, with the ratio (posterior spherical aberration)/(anterior spherical aberration) therefore shifting to compensate the positive spherical aberration of the cornea (-10%) in young subjects to add up aberration (26%) in old subjects. As for coma, these studies show the posterior corneal surface compensates approximately 3.5% the anterior surface coma, this compensation being larger for young subjects (6%) than for older subjects (0%). It can be therefore concluded that the posterior cornea has in general a small effect on high order aberrations of the eye, and that the slight compensation found in young eyes is lost with age (Dubbelman, Sicam & van der Heijde, 2007).

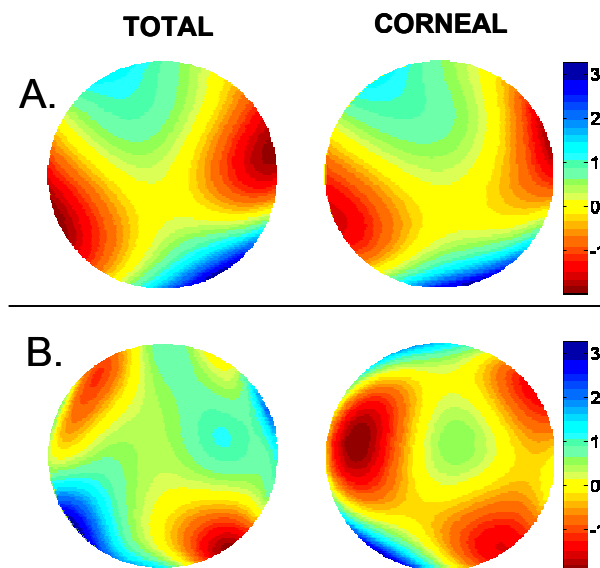


Figure 1.15. Total and corneal wave aberrations of both eyes of an unilateral aphakic 30-old patient. **A.** Aphakic eye (with no crystalline lens) and **B.** Normal contralateral eye. Note the similarity of corneal and total aberrations in the aphakic eye, and the compensation of corneal spherical aberration by the internal optics in the normal eye. Pupil diameter=6.5 mm. Figure adapted from Barbero (Barbero, Marcos & Merayo-Llodes, 2002b).

4.5 Interaction between Total and Corneal Aberrations:

The relative contribution of the cornea and crystalline lens to the overall ocular wave aberration is a relevant question in both the basic study of human eye optical quality and clinical ophthalmic applications. Although the magnitude and distribution of ocular aberrations differ substantially across subjects, a balance of corneal aberrations by internal optics, resulting in smaller ocular aberrations than those of the individual ocular components appears to be a common trend in young eyes.

The first reports of a compensation of corneal spherical aberration by the crystalline lens date back to the 70's, (El Hage & Berny, 1973, Millodot & Sivak, 1979). In a different study, Tomlinson (Tomlinson, Hemenger & Garriott, 1993) measured the contrast sensitivity of the eye for a small and large pupil size and using a knowledge of the expected aberration contribution from the cornea, predicted the aberration of the lens, finding positive values for the spherical aberration of the cornea, in the range 0-0.83 D, and negative spherical aberration of the crystalline lens, in the range 0 to -0.81 D. Similar findings were reported by Smith (Smith et al., 2001) who, as previously suggested by El Hage, measured the aberration of the whole eye, estimated the corneal aberration from the corneal shape, and from their difference reported a negative value of the spherical aberration of the lens approximately the same level as the positive value of the anterior corneal surface. Smith also studied the age effects on the spherical aberration and found that the older eye had much more total aberration than the younger eye while the aberration of the anterior corneal surface did not seem to be different between younger and older eye. In a recent study, Barbero (Barbero et al., 2002b) showed much higher spherical aberration in the aphakic eye of an unilateral aphakic young patient than in the normal eye, where corneal spherical aberration was reduced by the crystalline lens.

More recent studies have confirmed previous results on the balance of corneal and internal spherical aberration and also showed a reduction of corneal third-order coma by internal optics in young eyes. Artal (Artal & Guirao, 1998, Artal et al., 2001) found a significant coupling of individual aberration terms between the cornea and the internal ocular optics. Astigmatism for the cornea and internal optics (Zernike terms 3 and 5) had opposite signs, confirming the well-known fact in clinical practice that the internal optics tend to compensate for the corneal astigmatism. However, he found that this compensation also takes place for higher order aberrations. Third- and fourth-order

aberrations were also partially compensated. A large fraction of the spherical aberration of the cornea is cancelled by the internal optics. The magnitude of comalike aberrations of the cornea was also significantly reduced by the internal optics. Artal then opened the question whether this compensation was an active or passive process. In a later work, they showed that this compensation is larger in the less optically centered eyes (primarily hyperopic eyes), concluding that there was an auto-compensation mechanism that preserve the optical quality of the eye despite large variation in the ocular shape and geometry (Artal et al., 2006). Kelly (Kelly et al., 2004) in a study on 30 young subjects with relaxed accommodation, found strong evidence for compensation of horizontal/vertical astigmatism, lateral coma (for which they attributed an active compensation mechanism) and spherical aberration (which would occur passively). The active or passive nature of the compensation mechanism will be further addressed in this thesis in Chapter 9. This corneal/internal balance of spherical aberration and coma has been shown to be disrupted in older eyes (Artal et al., 2002), presumably because of structural changes in the crystalline lens, producing the reported increase of aberrations with age (Artal, 1993, Guirao, Gonzalez, Redondo, Geraghty, Norrby & Artal, 1999).

4.6 Misalignment of the ocular components

The eye is not a centered optical system. The fovea does not lie on the optical axis of the eye, and in fact, the optical axis of the ocular components cannot be defined. These commonly defined axes in the eye (Atchison & Smith, 2000b), which will be used in these thesis:

The *optical axis* is the line passing through the centers of curvature of the different surfaces of a centered system. Because the different surfaces of the eye are not centered to each other, this axis does not exist in the eye, although it has sometimes defined as the axis linking the center of curvature of the anterior corneal surface and that of the posterior lens surface.

The *line of sight* is the line joining the fixation point and the center of the entrance pupil. The position at which the line of sight intercepts the cornea is called the *corneal sighting center* (Mandell, 1995) or *visual center of the cornea* (Cline, Hofstetter & Griffin, 1989). Total aberrations measured (or simulated) in this thesis (Chapters 8 and 9) are referred to the line of sight.

The *visual axis* is defined by the line that joins the fixation target and the fovea position passing through the nodal points. It is sometimes referred to as the foveal achromatic axis, since it can be located by searching the pupil location that produces minimum transverse chromatic aberration for foveal fixation. The angle between the optical axis and the visual axis is the *angle alpha*.

Pupillary axis is defined by the line that passes through the center of the entrance pupil, which is normal to the cornea. The angle between the pupillary axis and the line of sight is defined as *angle lambda*. The angle between the pupillary axis and the visual axis is the *angle kappa*. In practical terms, angles kappa and lambda are the same. Lens tilt and decentration measurements reported in this thesis are referred to this axis (Chapters 2, 5, 8, and 9), except when the pupil was not available (iridectomized monkey eyes of Chapter 6).

The *Videokeratoscopic axis* is the axis of a keratometer or videokeratographic instrument, and it contains the center of curvature of the anterior cornea. In the standard operation of a corneal topographic instrument, the axis intercepts the line of sight at the fixation target. Corneal aberrations reported in this thesis are referred to the videokeratoscopic axis (Chapter 7) or the line of sight (Chapter 8).

4.7 Sources of optical aberrations in the normal eye: state of the art

The cornea and the crystalline lens are the major refractive components in the eye, and aberrations of the individual components are expected to contribute to overall image quality. Few studies address the sources of ocular aberrations from geometrical and optical structure of the individual components. Van Meeteren (van Meeteren & Dunnewold, 1983a) predicted, using schematic eye models, that tilt and misalignment of optical surfaces or a larger displacement of the fovea from the optical axis could give rise to both an increase in monochromatic aberrations (particularly astigmatism and coma) and an increase in optical transverse chromatic aberration (van Meeteren, 1974, van Meeteren & Dunnewold, 1983b). Marcos (Marcos et al., 2001) attempted to correlate the amount of misalignment of ocular surfaces and corneal shape with the amount of high order monochromatic aberrations of the eye (also transverse chromatic aberrations) in a group of 15 eyes, and concluded that simple relationships were not present. These are potential sources of optical aberrations that have been identified:

4.7.1. Ocular surface misalignments.

Early models in the literature Bennet and Rabbets (Bennett & Rabbetts, 1984) and van Meeteren (van Meeteren & Dunnewold, 1983a)) predicted that larger amounts of coma (van Meeteren & Dunnewold, 1983b) and TCA (Simonet & Campbell, 1990, Thibos, Bradley, Still, Zhang & Howarth, 1990) appear associated to large angle alpha. While those predictions were based on assumed average values, Marcos (Marcos et al, 2001) found that on an individual basis, the amount of coma (and TCA) was uncorrelated with the magnitude of angle alpha. This could be explained by a compensation of corneal horizontal coma by the internal optics, as demonstrated by Artal (Artal et al., 2006).

4.7.2. Pupil Centration.

Simple models show that pupil decentration causes an increase in the monochromatic aberrations (van Meeteren & Dunnewold, 1983b, Walsh & Charman, 1988) and in transverse chromatic aberration (Artal, Marcos, Iglesias & Green, 1996, Bradley, Thibos, Zhang & Ye, 1991, Thibos, 1987, Thibos et al., 1990), which produce a degradation in the retinal image (Artal et al., 1996, van Meeteren & Dunnewold, 1983b). Eye models proposed by Atchison and Smith, based on on-axis, rotationally symmetric components, predict that coma will be produced if the pupil is decentered (Atchison & Smith, 2000a). However, although it is clear that a systematic pupil decentration will increase retinal image degradation, and this has been experimentally demonstrated (Artal et al., 1996), typical pupil decentration occurring in normal eyes does not appear to be a major contributor to coma. Marcos (Marcos et al., 2001) did not find any correlation between pupil decentration and coma or TCA. Also, pupil shifts with pupil dilation have been reported to be small (Yabo, Thompson & Burns, 2002).

4.7.3. Corneal shape, corneal irregularities and refractive index

The effect of anterior corneal shape and irregularities on corneal aberrations has been discussed in section 4.4. The contribution of the corneal posterior surface to the overall aberrations has been shown to be limited in the normal eye (as discussed in section 4.4.), and to play a moderate compensatory role, particularly on astigmatism, spherical aberration and coma terms (as discussed in section 4.5) (Dubbelman et al., 2007, Dubbelman et al., 2006, Sicam et al., 2006)

Recent studies address the potential role on the refractive power of the cornea of the differences in refractive index of the different corneal layers and tear film (including a gradient index structure in the stroma) (Barbero, 2006). The effect of using a multilayer cornea (rather than an average refractive index) on high order aberrations has not been addressed but it is likely to be small.

4.7.4. Crystalline lens shape, structure and refractive index.

As it has been reported in sections 2.4.1, spherical aberration of the young crystalline lens is negative (Artal & Guirao, 1998, Artal et al., 2001, El Hage & Berny, 1973, Kelly et al., 2004, Sivak & Kreuzer, 1983, Smith et al., 2001, Tomlinson et al., 1993). Lens radius of curvature, asphericity and gradient index contribute to the final value of the spherical aberration (Artal et al., 2002). As has been presented in 2.4, all these factors are age dependent although there are controversial data in the literature on the magnitude and rate of these changes. The influence of the changes of lens radii of curvature with age on refraction (particularly in relationship with the lens paradox) have been studied (Dubbelman & van der Heijde, 2001, Koretz & Handelman, 1986a). However, the impact of individual lens geometry and structure on high order aberration has not been addressed, in part because of the lack of knowledge on the gradient index structure.

Another potential source of lens irregularities are the crystalline lens sutures. Some scatter and refractive changes occur at the suture points, especially along the optical axis of the lens, as it has been demonstrated by Kuszak (Kuszak, 2004, Kuszak, Peterson, Sivak & Herbert, 1994) in primate lenses. This study found that focal variability was least when the beam was passed through uniformly hexagonal fibers aligned along the optical axis, and greatest when the beam passed through irregularly-sized and shaped fibers ends arranged as suture branches within growth shell and suture planes aligned along the optical axis. Significant amount of total trefoil measured in vivo has often been attributed to the lens sutures both in humans (Thibos et al., 2000) and monkeys (Ramamirtham, Kee, Hung, Qiao-Grider, Roorda & Smith, 2006), and have been shown to play an impact on retinal image quality (Navarro & Losada, 1997).

5. THE OPTICAL QUALITY OF THE PSEUDOPHAKIC EYE

5.1 Cataract surgery

Metabolic changes of the crystalline lens fibers over time lead to the development of a loss of transparency producing an opacification, is called cataract. Cataract surgery consists of the removal of the lens that has developed this opacification. There are different types of surgery, the most used methods, are phacoemulsification and extracapsular cataract extraction: 1) *Phacoemulsification*. It involves the use of a machine with an ultrasonic handpiece with a titanium or steel tip. The tip vibrates at ultrasonic frequency (40.000 Hz) and the lens material is emulsified. Fragmentation into smaller pieces makes emulsification easier, as well as the aspiration of cortical material (soft part of the lens around the nucleus). After phacoemulsification of the lens nucleus and cortical material is completed, a dual irrigation-aspiration (I-A) probe or a bimanual I-A system is used to aspirate out the remaining peripheral cortical material. All cataract surgeries reported in this thesis were performed using this technique. 2) *Extracapsular cataract extraction (ECCE)*: It involves manual extraction of the lens through a large (usually 10-12 mm) incision made in the cornea or sclera. Although it requires a larger incision and the use of stitches, the conventional method may be indicated for patients with very hard cataracts or other situations in which phacoemulsification is problematic. None of the cataract surgeries reported in this thesis were performed using ECCE, but some of the literature results presented for comparison were. After cataract extraction, a foldable intraocular lens is introduced through the incision; once inside the eye, the lens unfolds to take position inside the capsule.

Figure 1.16 shows a scheme of a typical procedure for cataract surgery.

Introduction

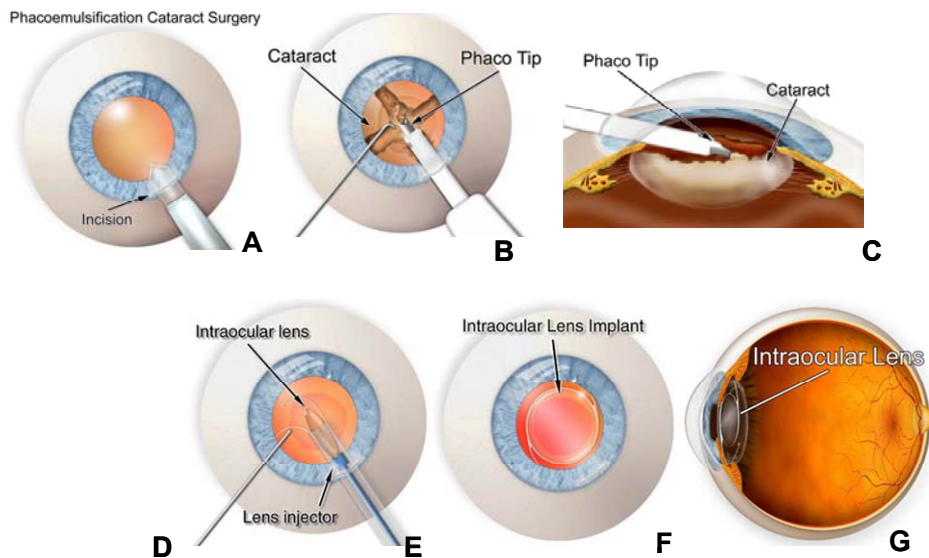


Figure 1.16. Illustration of the cataract surgery procedure. **A.** Incision. All the surgeries reported in this thesis used 3.2-mm superior incisions. **B.** Capsulorhexis: The surgeon creates an opening in the capsule. **C.** Phacoemulsification. Ultrasonic vibrations are used to break the cataract into smaller fragments that are then aspirated from the eye using the same instrumentation. **D.** Creation of grooves in the cataract. **E.** Once the denser central nucleus of the cataract has been removed, the softer peripheral cortex of the cataract is removed using an irrigation/aspiration handpiece. The posterior or back side of the lens capsule is left intact to help support the intraocular lens implant. **F.** Injection of the intraocular lens. **G.** Intraocular lens implanted.

5.2 New designs of intraocular lenses.

Since 1949, when Ridley first introduced an artificial intraocular lens (IOL), the design and material used to make the IOL has been in a continuous evolution to find the ideal IOL design to minimize decentration, dislocation, optical aberrations and the most biocompatible material (Doan, Olson & Mamalis, 2002). The original IOL that Ridley implanted was made of rigid polymethyl methacrylate (PMMA), inserted through an extracapsular route with a relatively large wound inducing postoperative astigmatism, with a long healing process and slow recovery despite the proven biocompatibility. Since then, significant advances have been made in materials that reduce the risk of posterior capsule opacification (i.e. hydrophobic acrylic and some silicone materials (Hayashi, Hayashi & Nakao, 1998)) can be easily folded, and allow thinner optics and therefore smaller wound size due to their higher indices of refraction. Efforts have also been directed to better haptic designs, and multiple designs are available either as single piece or three piece-IOLs. The design of the haptics is critical to prevent forces that may cause capsular bag contraction, leading to movement, rotation, tilt and decentration

(Faucher & Rootman, 2001, Petersen, Bluth & Campion, 2000). Another important aspect of the design affects the IOL edge. For example, it is well known that squared edges create a capsular bend that stops the posterior capsular opacification (Nishi, Nishi & Akura, 2001, Schmack & Gerstmeyer, 2000), but allow for reflection of light internally producing higher rate of glare (Ellis, 2001, Farbowitz, Zabriskie & Crandall, 2000). Newer designs have a frosted edged or rounded anterior edge to prevent the formation of those images. Finally, the most critical design parameter affecting retinal image quality is the shape of the IOL surfaces (radii of curvature, asphericities and shape factor for monofocal lenses (Barbero & Marcos, 2007, Tabenero, Piers & Artal, 2007), and more complex relationships in multifocal or pseudo-acomodative IOLs. A major goal in current cataract refractive surgery is to achieve ametropia (with monofocal designs), or extended range of focus in multifocal or pseudo-accommodative designs. In this regard, accurate ocular biometry and reliable methods to determine the required IOL power are essential. A good control of high order aberrations with IOLs will allow to improve those primary goals and optimise retinal image quality.

5.2.1 Monofocal Intraocular lenses: spherical and aspheric surfaces

Monofocal IOLs attempt to produce optimal retinal image quality at a single plane of focus (generally infinity). Until recently, most common designs exhibited spherical anterior and posterior surfaces. Spherical IOLs show inherent spherical aberration, which generally adds up to the spherical aberration of the cornea, which as described in 4.4 is typically positive. Still, an appropriate choice of design parameters of spherical IOLs can optimise retinal image quality (spherical aberration in combination with defocus) (Barbero & Marcos, 2007). The advantages of having a finite amount of residual positive spherical aberration are known to include: an increased depth of focus (Marcos et al., 2005) , which in certain circumstances may partially compensate for loss of accommodation in a presbyopic eye; positive spherical aberration may help patients with hyperopic postoperative refraction; and modest amounts of positive spherical aberration may mitigate the adverse effects of chromatic aberration and higher order monochromatic aberrations (McLellan, Marcos, Prieto & Burns, 2002) .

Examples of spherical IOLs used in this thesis are Acrysof SA60AT (Alcon) or Ceeon 912 (Pharmacia).

Aspheric IOLs have a controlled amount of inherent negative spherical aberration and mimics that of a healthy natural crystalline lens in a relaxed state.

Examples of the aspheric intraocular lenses used in this thesis are the Tecnis Z9000 (AMO) IOL (Altmann, 2005), made of silicone, refractive index of 1.458, with an anterior aspheric surface, and Acrysof IQ (Alcon) with a posterior aspheric surface. Figure 1.17 shows aberrations patterns in eyes after implantation of spherical and aspheric intraocular lenses.

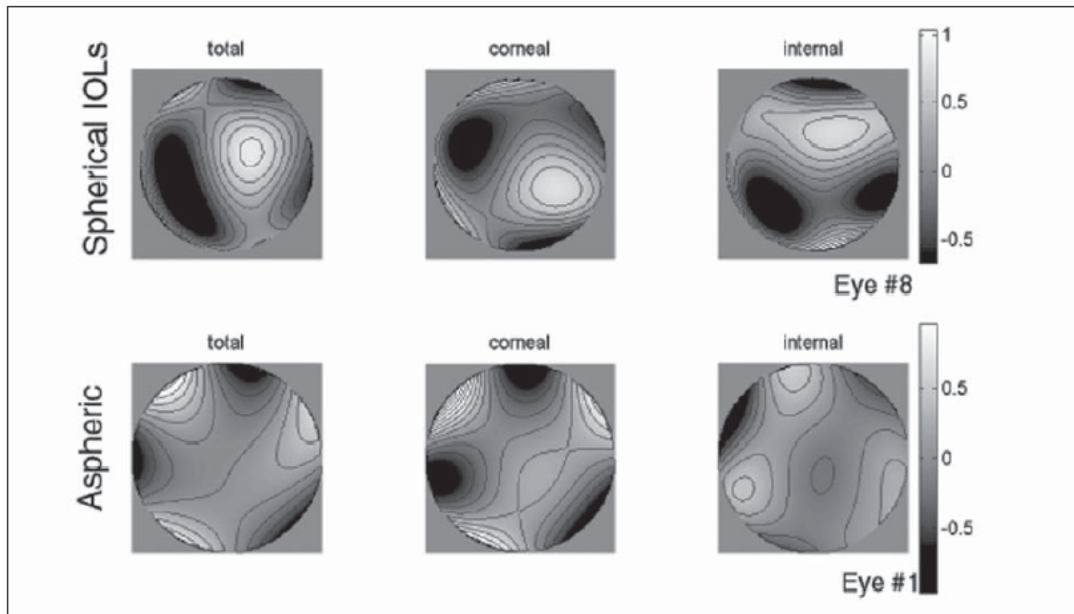


Figure 1.17. Example of corneal, internal and total aberration patterns (referred to the pupil center) in eyes after implantation of spherical and aspheric intraocular lenses adapted from Marcos (Marcos, Barbero & Jiménez-Alfaro, 2005). Pupil diameter: 4.5 mm).

5.2.2. Multifocal Intraocular Lenses

As opposed to monofocal IOLs, multifocal IOLs (McDonald, 2003) attempt to provide usable vision at various focal planes (far, intermediate, or near). In general, they are based on two possible different approaches: 1) *Refractive multifocal IOLs* show different refractive concentric zones, some of which focus light from near objects, some from intermediate objects and some from distance objects that distributes light over the optical zones to provide near, intermediate, and distance vision. 2) *Diffraction Multifocal IOL* (Lee & Simpson, 1997) are diffractive optic elements that produce typically two foci, one for near and the other one for far vision (with light intensity distribution dependent on the design). Other designs (Altmann, Nichamin, Lane & Pepose, 2005) combine a diffractive design with central and peripheral refractive areas.

None of the experiments presented in this thesis involves patients with multifocal IOLs, but some of the techniques developed (i.e. IOL tilt and decentration measurements with Purkinje imaging) could be applied to this case (of particular relevance to refractive multifocal IOLs with multiple bands, which rely on an accurate centration).

5.2.3. Accommodative lenses

Accommodating intraocular lens (IOL) assemblies have been developed that comprise an IOL that moves in response to ciliary muscular contraction and relaxation, thereby to simulate the movement of the natural lens in the eye, and, inter alia, help provide patients with better focusing ability (Israel, 2003).

There are several types of accommodative intraocular lenses, including: 1) *Single-optic accommodative lens designs* The mechanism of action is based on the concept of relaxation of zonular fibers with contraction of the ciliary body, leading to relaxation of the capsular bag and forward movement of the intraocular lens at the hinged haptics (Helmholtz theory); 2) *Two-optic accommodative lens design* (Peng, Yang & Zhang, 2005) with two lenses that move relative to each other along the optical axis of the lens system in reaction to movement of the ciliary muscle.

None of the experiments presented in this thesis involves patients with accommodative IOLs, but some of the techniques developed (i.e. IOL tilt and decentration measurements with Purkinje imaging) could be applied to this case (of particular relevance due to the moving nature of these lenses). Also, the customized computer model eyes developed in these thesis could be used to accurately predict their optical performance.

5.2.4 Other innovative pseudophakic IOL designs

Multiple IOL approaches are still under investigation or clinical trials. Based on the innovation and potential, we highlight 1) *Light Adjustable IOLs*: The LAL is a photosensitive silicone intraocular lens whose power can be adjusted noninvasively and cured after implantation using a low-power light source. It is primarily devised as a monofocal implant, and other than focus, higher order aberrations could be optimised (i.e. correcting post-operatively corneal aberrations). The technology developed in this thesis is well suited for the in vivo characterization of this devices. 2) Hydrophobic acrylic gel polymer (Ho, Erickson, Manns & Parel, 2006), as a method to restore

accommodation using a thermodynamic material sensible to the changes of temperature that would replace the crystalline lens material and could be dynamically reshaped by the capsule, as in a young crystalline lens. The phakometry techniques developed in this thesis are ideal to fully characterize the changes in lens curvature with this implanted material in vivo.

5.2.5. Phakic lenses

Typically designed to correct high myopia in young patients, phakic IOLs (Tran & van Noy, 2003), unlike in clear lens extraction, are implanted without removal of the crystalline lens of the eye. Patients undergoing this procedure can retain any pre-existing focusing ability. In the phakic IOL procedure, a lens, made of plastic or silicone, is placed inside the eye. There are three designs under development (IOLs placed in front of the iris, iris claw lens, attached on the front of the iris and so-called Implantable Contact Lens, or ICL placed between the iris and crystalline lens). We have not included this type of implant in this thesis, but the technology developed could be equally applied to these cases.

5.3 Optical quality of eyes after cataract surgery.

The advances produced in cataract surgery, particularly foldable intraocular lenses that allow implantation through small incisions, or more sophisticated optical surfaces will definitely have an impact on the optical outcomes. To evaluate optical quality of eyes after cataract surgery is important to study the efficiency of those new designs.

Double-pass retinal image quality was first used to evaluate objectively optical quality after cataract surgery (Artal, Marcos, Navarro, Miranda & Ferro, 1995, Hayashi, Hayashi, Nakao & Hayashi, 2000, Guirao et al., 2002). This technique was used to compare optical performance and depth-of-field between multi- and monofocal IOLs (Artal et al., 1995). Also, a comparison of the double pass retinal quality of patients after cataract surgery with an age matched control group, and with healthy young subjects, showed that pseudophakic eyes' optical quality was worse than of healthy younger subjects. This suggests that factors associated to the implantation, the design of the lens, and the lack of aberration coupling in eyes with IOLs (as opposed to young crystalline lenses) contributed to optical image degradation.

Barbero (Barbero et al., 2003) measured for the first time in vivo corneal, total and internal aberrations of patients after cataract surgery. Measurements of the aberrations of the individual optical components allowed better identify sources of optical aberrations. This study showed (as later reported in more eyes in a study by Guirao (Guirao, Tejedor & Artal, 2004) and another study presented in Chapter 7 of this thesis) a slight increase in corneal aberrations due to the incision.

More recently, studies on ocular aberrations and visual performance with newer IOL designs have been presented. Marcos (Marcos et al., 2005) in a comparative study of patients with spherical and aspherical IOLs implanted (Holladay, Piers, Koranyi, van der Mooren & Norrby, 2002), found that eyes with aspheric IOLs showed spherical aberration not significantly different from zero. However, tolerance to defocus was lower in these eyes (Marcos et al., 2005, Rocha, Soriano, Chalita, Yamada, Bottós, Bottós, Morimoto & Nosé, 2006). Recent studies have addressed ocular aberrations in eyes with other types of IOLs (Chung, Lee, Lee, Seo & Kim, 2007)

While the description of the optical performance in eyes with IOLs is interesting, as it can provide insights on the visual quality of the patients, the identification of the sources of these measured optical aberrations is essential to improve surgery and IOL designs. Chapters 7, 8 and 9 of this thesis will address the measurement and understanding of the impact of each factor contributing to optical performance in pseudophakic eyes and relating those to the ocular aberrations measured on these eyes.

6. HYPOTHESIS AND GOALS OF THIS THESIS

Our hypothesis is that knowledge of the crystalline lens/intraocular lens geometry and positioning will help us to better understand the optical quality of the normal and pseudophakic eye and accommodative mechanism of the eye. We will test this hypothesis by measuring crystalline lens curvature, tilt and decentration (with Purkinje and Scheimpflug imaging techniques implemented and validated in this thesis) in young human eyes and Rhesus Monkeys, and by measuring IOL tilt and decentration, ocular surface misalignments and corneal changes in eyes after cataract surgery. With the aid of customized computer eye models we will be able to predict the role of each factor to optical aberrations.

The specific goals of this thesis are:

1.- Development of custom technology, based on Purkinje imaging, to measure phakometry and tilt and decentration of the lens in vivo (Chapter 2).

2.- Implementation of processing algorithms for Scheimpflug images of the anterior segment of the eye to obtain lens shape and position (Chapter 3).

3.- Computer and experimental validations of the technology developed in this thesis, to test the assumptions and reliability of the techniques (Chapters 2, 4 and 5)

4.- Investigation of the radii of curvature and tilt and decentration of the crystalline lens in normal young human eyes in vivo, and their changes with accommodation (Chapter 4).

5.- Investigation of the changes in radii of curvature of the anterior and posterior crystalline lens surfaces and lens tilt and decentration with accommodation in vivo, in a rhesus monkey experimental model (Chapter 6).

6.- Assessment of the lens tilt and decentration (in two dimensions) in patients implanted with intraocular lenses (Chapter 2, 8 and 9).

7.- Evaluation of the changes induced by incision in cataract surgery measuring patients before and after implantation of intraocular lenses (Chapter 7).

8.- Study of the accuracy of computer eye models to predict ocular aberrations, in comparison with ocular aberrations measured on the same patients (Chapter 8)

9.- Quantification of the relative contribution of factors contributing to optical aberrations in patients implanted with intraocular lenses: corneal topography, intraocular lens geometry, lens tilt and decentration and line-of sight misalignment, using customized computer eye models, (Chapter 8).

10.- Investigation of the effect of tilt and decentration of the lens on the optical quality of the eye, and the passive or active nature of cornea and lens compensation mechanism in the human eye (Chapter 9).